New Jersey Institute of Technology

Digital Commons @ NJIT

Fall 1-31-1996

Linearly tapered slot antenna

Luis Alberto Tumialan
New Jersey Institute of Technology

ABSTRACT

LINEARLY TAPERED SLOT ANTENNA

by
Luis Alberto Tumialan

Design procedure for Linearly Tapered Slot Antennas (LTSA) has been developed

and implemented using High Frequency Structure Simulator (HFSS) code based on a

finite-element analysis.

A CAD study of two variations of a LTSA based on either a stripline or a

microstrip feed has been carried out. Circular and radial stubs have been considered in

these designs for an antenna operating at 10 Ghz. LTSA on a Duroid substrate fed by a

stripline has been designed to operate with better than 12 dB return loss. Fabricated

antenna was characterized and had even a wider response than the CAD design. Radiation

patterns also were measured for this antenna. Furthermore, microstripline-fed LTSA

designs were made. Further work on a low temperature co-fired ceramic substrate LTSA

antennas and their arrays has been suggested.

LINEARLY TAPERED SLOT ANTENNA

by
Luis Alberto Tumialan

A Thesis
Submitted to the Faculty of
New Jersey Institute of Technology
in Partial Fulfillment of the Requirements for the Degree of
Master of Science in Electrical Engineering

Department of Electrical and Computer Engineering

January 1996

APPROVAL PAGE

LINEARLY TAPERED SLOT ANTENNA

Luis Alberto Tumialan

Dr. Edip Niver, Thesis Advisor   Date
Associate Professor of Electrical Engineering, NJIT

Dr. Gerald Whitman, Committee Member   /   Date
Professor of Electrical Engineering and Director
of the Center for Microwave and Lightwave Engineering, NJIT

Dr. Sol Rosenstark, Committee Member   Date
Professor of Electrical and Computer Engineering, NJIT

BIOGRAPHICAL SKETCH

Author: Luis A. Tumialan

Degree: Master of Science in Electrical Engineering

Date: December 1995

Undergraduate and Graduate Education :

Master of Science in Electrical Engineering
New Jersey Institute of Technology, Newark, NJ, 1995

Bachelor of Science in Electrical Engineering
National University of Engineering, Lima, Peru, 1980

Major : Electrical Engineering

ACKNOWLEDGMENT

TABLE OF CONTENTS

LIST OF TABLES

LIST OF FIGURES

LIST OF FIGURES
(Continued)

CHAPTER 1

INTRODUCTION

Planar antennas constitute an important class of practical antennas. The general classification of antennas in terms of broadside and endfire radiation is equally applicable to planar antennas. The broadside planar antenna radiates in a direction normal to the surface of the antenna plane, while the endfire antenna radiates along the plane of the radiating element. Typical example for a broadside planar radiator is a microstrip patch. The subject of this thesis, tapered slot antenna (TSA) is a good example of an endfire planar radiator.

The attractiveness of planar antennas is due to their easy integration to monolithic manufacturing technologies and relatively low cost with respect to their competing counterparts, low profile and light weight. They are currently applied in many diverse applications, such as, mobile communications, global positioning systems (GPS), intelligent vehicle highway systems (IVHS), remote sensing, plasma diagnosis, radar and many more. All these applications cover a wide spectrum extending from sub GHz to THz frequencies.

The tapered slot antenna, in addition to its endfire radiation capability, offers other attractive features, such as, narrower beamwidth, wider bandwidth, and higher gain in comparison to the patch radiators. Furthermore, tapered slot antenna arrays can be configured as 2-D arrays where the endfire direction is used for radiation and the other.

1
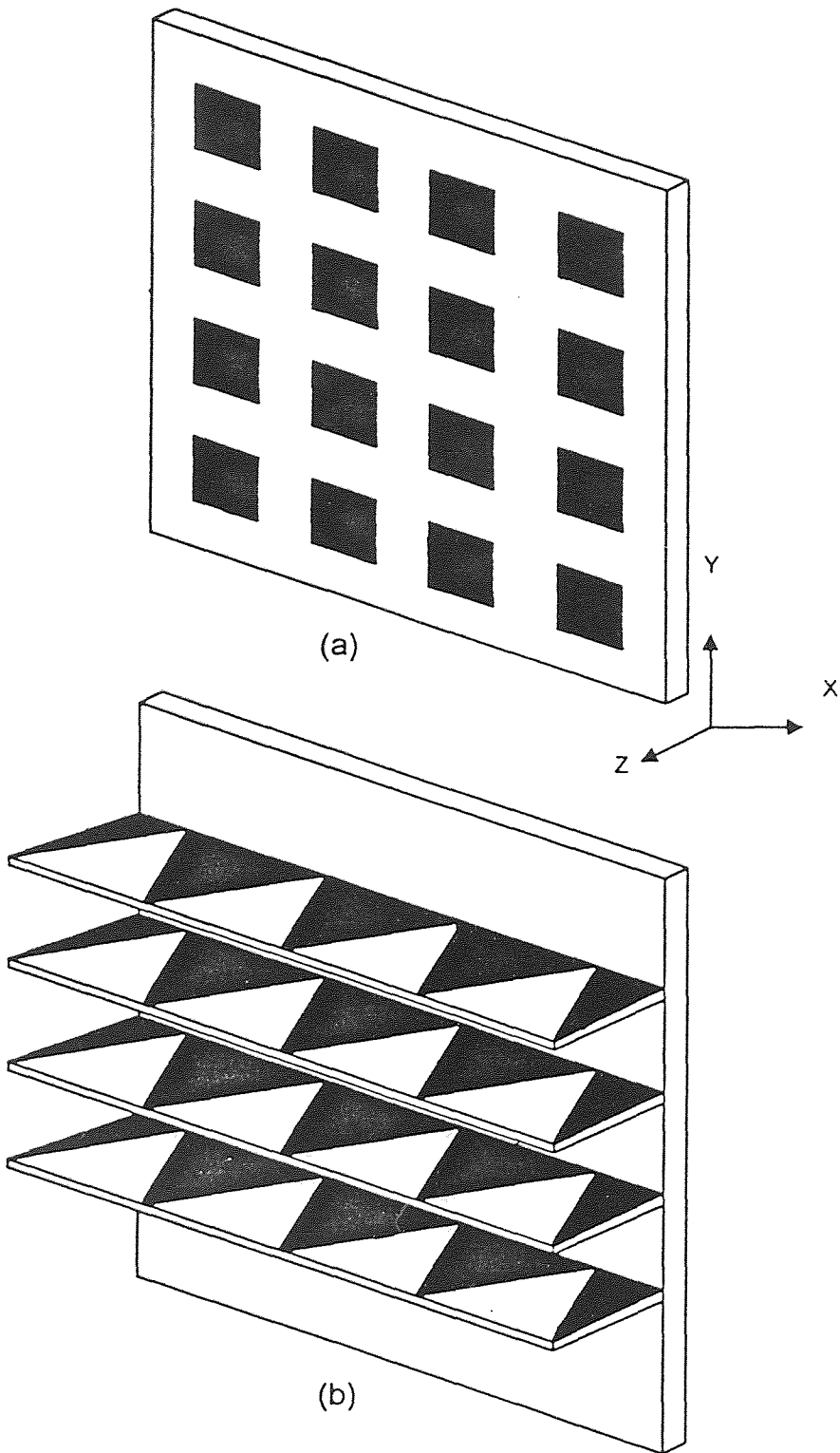
Figure 1. Types of 2-D planar antenna arrays
(a) Broadside Antenna Array ;
(b) Endfire Antenna Array.

comparison to the patch radiators. Furthermore, tapered slot antenna arrays can be configured as 2-D arrays where the endfire direction is used for radiation and the other transversal direction is for the layout of array components, such, as phase shifters, active components, etc

The ease of fabrication of tapered slot antennas combined with their attractive performance features have produced diverse applications such as:

- 94 Ghz Cassegrain seven-element linearly tapered slot antenna (LTSA) imaging system [1],
- planar Gunn oscillator with a TSA at 35 Ghz [2],
- 21-element Ka-Band phased array using MMIC devices and Vivaldi antennas at 32 Ghz [3].

This thesis presents the CAD analysis of a LTSA antenna at 10 Ghz for a teflon woven substrate (Duroid). This antenna was fabricated on the Duroid substrate and was characterized.

CHAPTER 2

TRAVELING-WAVE ANTENNAS

The performance characteristics of a linearly tapered slot antenna (LTSA) can be understood by studying traveling-wave antennas.

2.1 Traveling-wave antennas

In traveling-wave antennas, the current distribution can be synthesized in terms of waves propagating in only one direction, i.e., in the forward waves; reflected waves are usually neglected due to their insignificant contribution. This behaviour is quite opposite compared to standing wave or resonant antennas, where the current distribution the superposition of forward and reverse waves along the antenna. Typical antenna types shown in Figure 2 representing traveling-wave antennas are usually many wavelengths in size, whereas resonance antennas are limited in size, i.e., to $\lambda/2$, etc. Traveling-wave antennas usually offer low profile and simplicity in the feed structures. In general, they are classified into two main types [4]:

- Leaky-wave Antennas ($v_{ph,z}/c > 1$),

- Surface-wave Antennas ($v_{ph,z}/c < 1$).
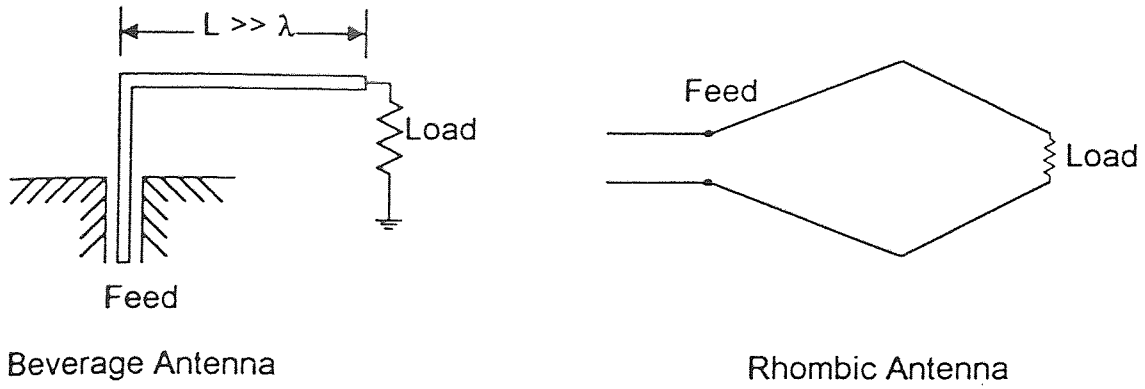
(a) Traveling-wave antennas
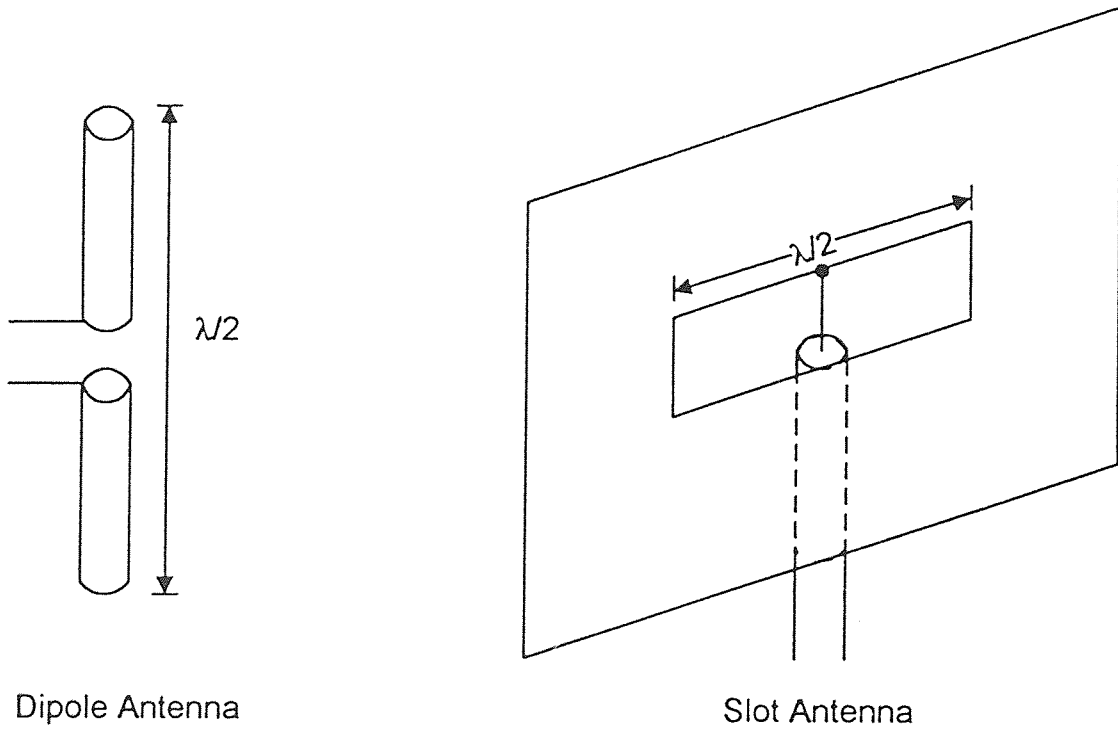
(b) Resonant antennas

Figure 2. Typical antenna types.

Leaky-wave antennas are based on the leakage of energy continuously along the antenna structure and, in general, produce broadside radiation. Since endfire radiation is associated with LTSA structures, the discussion of traveling-wave antennas will be limited to surface-wave antennas.

2.2. Surface-wave Antennas

A surface-wave is defined by Barlow and Brown [5] as a wave

> "that propagates along an interface between two different media without radiation; such radiation being construed to mean energy converted from the surface-wave field to some other form."

From this definition, it is observed that contrary to the continuous electromagnetic radiation of a leaky-wave, a surface-wave is bound to the surface and radiation exists only at curvatures, nonuniformities, and discontinuities. As a consequence, the total radiation pattern of a uniform surface-wave antenna is determined by the feed and termination properties. Using the separability property of the 2-dimensional wave equation and defining the propagation constant such that it represents a surface-wave, i.e., parallel propagation along the interface ($\beta_z \neq 0$, $\beta_x=0$) and vertical decay to it ($\alpha_x>0$), one can deduce the following relationship:

$$\frac{\beta_z}{k_0} = \frac{c}{v_{ph,z}} = \sqrt{1+\left(\frac{\alpha_x \lambda_0}{2\pi}\right)^2} > 1 \qquad (1)$$

An actual design of surface-wave antennas requires the use of tapers to smooth the transition between the differents parts of the antenna while preserving the conditions for the existence of the surface-waves. Using Figure 3 as an example, there is a taper between the feed F and the antenna structure which permits the coupling of a portion of the input power to the surface wave. At the terminal end of the structure (T), there is another taper which is used to reduce the otherwise abrupt termination so as it does not affect the pattern and bandwidth of the antenna significantly. The optimum design of these antennas should permit the generated surface wave to illuminate the terminal aperture(perpendicular plane at the end of the antenna) in the largest possible area to produce the optimum gain. This is achievable by ensuring that the transverse attenuation of the surface wave α_x at the terminal, is the smallest possible value that will comply with (1). As a consequence, the optimum ratio v_{ph}/c will yield values near to unity. Since the surface-wave phase front is in the aperture plane, the radiation pattern has its maximum in the endfire direction. The radiation characteristics of these antennas pinpoint their usefulness in applications which require endfire radiation and low-profile design,e.g., flush-mounted aircraft and missile antennas.

Design parameters of surface-wave antennas

Antenna directivity can be defined as

$$D = \frac{4\pi|F(\theta,\phi)_{max}|^2}{\int_0^{2\pi}\int_0^{\pi}|F(\theta,\phi)|^2 \sin\theta d\theta d\phi} \tag{2}$$
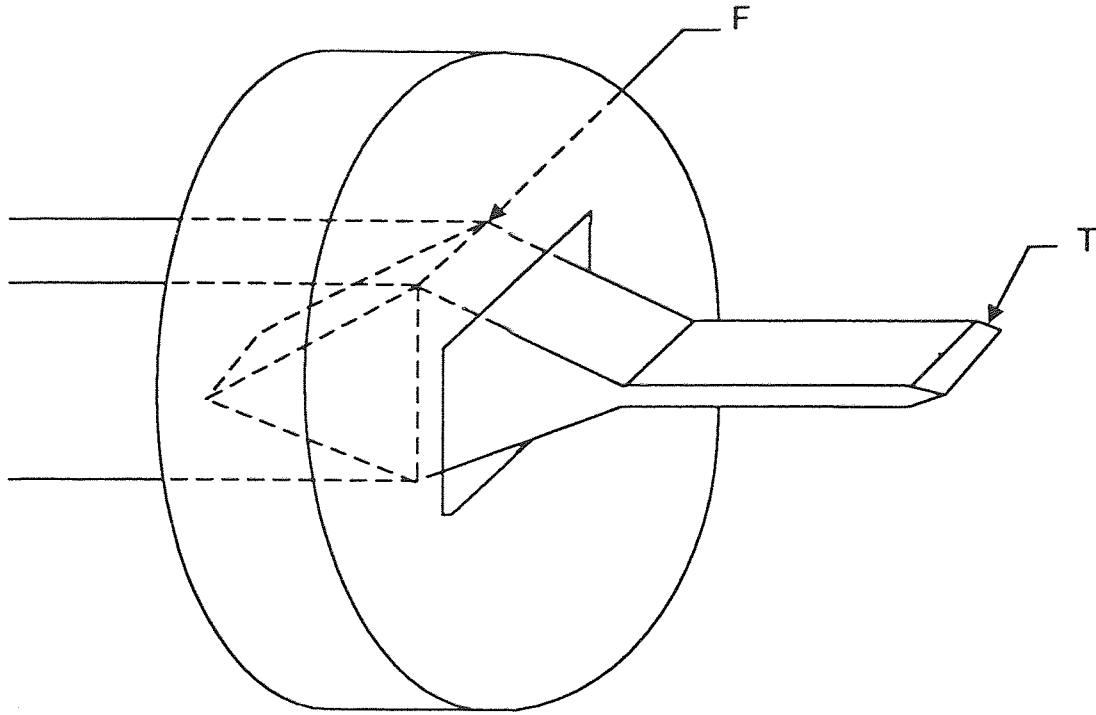
Figure 3. Dielectric rod antenna with rectangular cross-section.

where $F(\theta,\phi)$ is the far-field pattern factor of an antenna. From (2), the directivity of a uniform line source of length L is deduced as [5]

$$D = \frac{2\left\{\dfrac{\sin[(k-\beta)L/2]}{(k-\beta)L/2}\right\}}{\displaystyle\int_{-1}^{1}\left\{\dfrac{\sin[(k-\beta)L/2]}{(k-\beta)L/2}\right\}d(\cos\theta)} \qquad (3)$$

where k is the wavenumber in the medium, i.e., $k=2\pi/\lambda$ and β is the phase change coefficient along the antenna. Variations of relative directivity $D/(L/\lambda)$ as a function of the relative length L/λ, and phase velocity v_{ph} based on (3) are shown in Figure 4. It is observed from this graph that the directivity of a uniform line source in the broadside direction, and even for any angle of radiation approaching the endfire direction, is equal to $D \approx 2\,L/\lambda$ provided $L/\lambda \gg 1$; L is the length of the antenna. In the endfire direction, the directivity increases to $D \approx 4L/\lambda$.

Hansen and Woodyard [7] using the expression (3) determined the optimum directivity for the uniform line source $(L \gg \lambda)$, by adjusting the phase velocity $v_{ph,z}$. From this study, it was established that in order to get the optimum D there must be a phase difference of approximately 180° between the surface wave and the free-space wave over the total length of the antenna, i.e.,

$$\beta_z L = \pi + kL \qquad (4)$$

or,

$$c/v_{ph} = 1 + \lambda/(2L) \qquad (5)$$
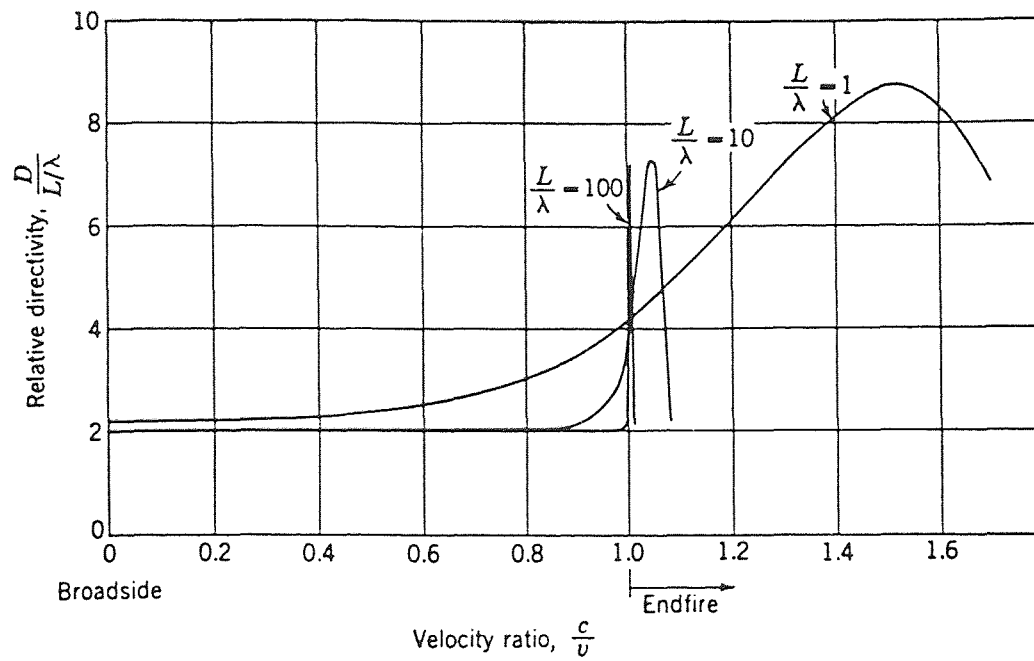
Figure 4. Relative directivity as a function of length and phase velocity.

For this case, the optimum directivity is (see Figure 4):

$$D \approx 7L/\lambda \qquad (6)$$

More experimental data useful for these antennas, but of shorter lengths, were gathered and analyzed by Ehrenspeck and Poehler [8]. They found that for antennas lengths less than 20λ, the phase difference necessary for optimum gain can be shorter than the $180°$ required by the Hansen-Woodyard criteria. This phase increase is around $60°$ for antennas of 1λ, and it increases to $120°$ for antenna lengths between 4λ and 8λ, and, in the extreme case, it tends to the Hansen-Woodyard condition for much longer antenna of 20λ. The criteria mentioned above can be reduced to the following single expression:

$$c/v_{ph} = 1 + \lambda/(pL) \qquad (7)$$

with p being 6 for $L=\lambda$, 3 for L between 4λ and 8λ, and to 2 at 20λ. In the case in which the launching efficiency is high, the only concern for getting the surface-wave established would be that the length L surpasses L_{min} [9], i.e.,

$$c/v_{ph} = 1 + \lambda/(6L) \qquad (8)$$

All these conditions for optimum gain are represented in Figure 5, which depicts the curves of c/v_{ph} as a function of the ratio of the antenna length relative to wavelength
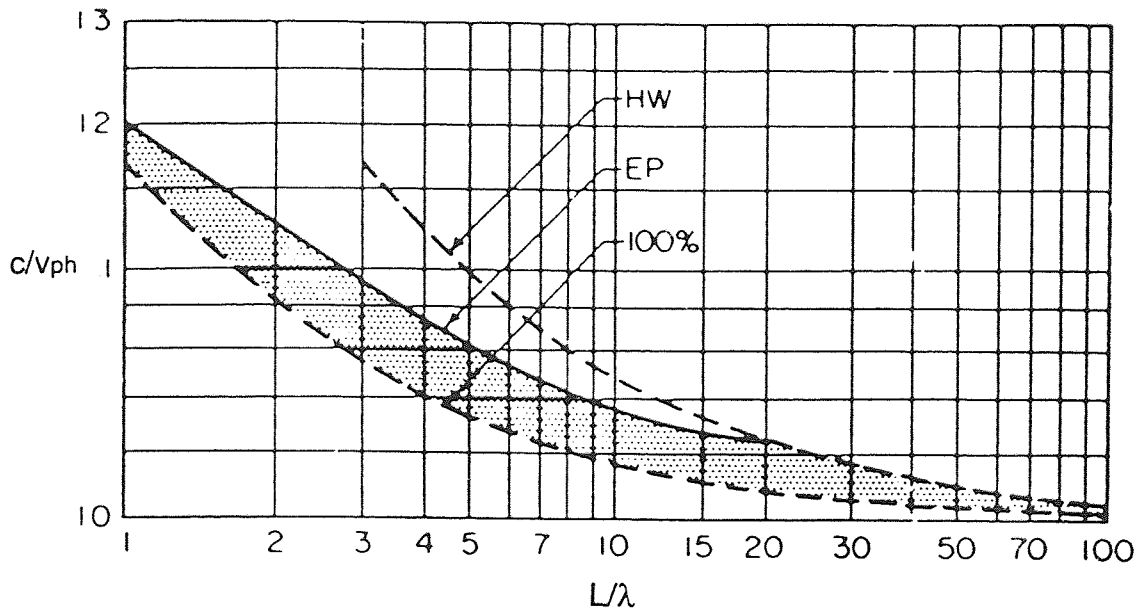
Figure 5. Relative-phase velocity c/vph as a function of relative antenna length L/λ for maximum gain surface-wave. HW = Hansen-Woodyard condition; EP = Ehrenspeck and Poehler experimental data; 100 % = idealized perfect excitation [7].

The lowest ordinate represents the ordinary endfire condition ($c/v_{ph}=1$). For optimum gain endfire antennas, the expression(6) is good for antenna lengths between 10λ to 50λ. For longer lenghts ($L>50\lambda$), an adequate value is

$$D \approx 4L/\lambda \qquad (9)$$

and for lengths between 3λ and 8λ

$$D \approx 10L/\lambda \qquad (10)$$

Zucker[7], using the above information and reported data in an open literature, plotted Figure 6, where the solid lines indicate the optimum gain and beamwidth, while the dashed lines represent broad bandwidth and low sidelobe level. The half-power beamwidth BW in the maximum-gain case is approximated by the following expression

$$BW \cong 55\sqrt{L/\lambda} \qquad (11)$$

Normally the beamwidth is slightly smaller in the E-plane and larger in the H-plane. Figures 5 and 6 jointly with some design principles suggested by Zucker [9] are normally referred to as Zucker's design principles for surface-wave antennas of maximum-gain; they have been successfully applied to the study of many antennas such as: millimeter-wave dielectric tapered rod antennas [10] , and tapered slot antennas [11].
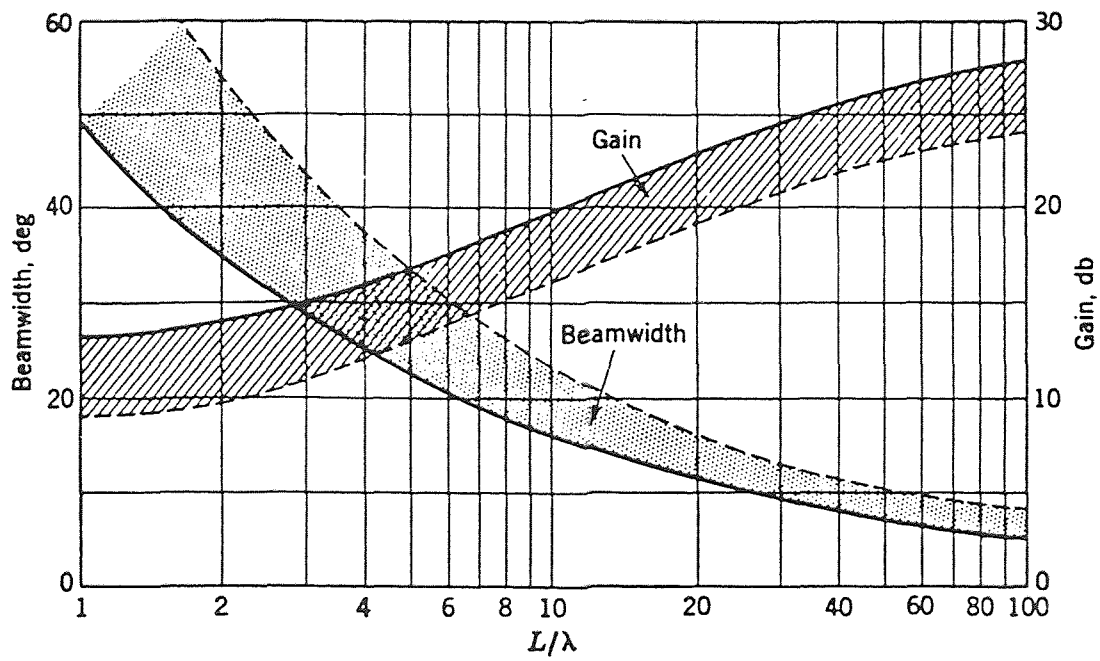
Figure 6. Gain and beamwidth of a surface-wave antenna as a function of relative length L/λ. Solid lines are optimum value and dashed lines are for low sidelobe and broadband design [7].

CHAPTER 3

TAPERED SLOT ANTENNA

The overall performance of any radiating system strongly depends on the efficient coupling of the source to the radiating element. The radiation problem of the source and radiating element connection via the feed structure remains a challenging boundary value problem in terms of securing a rigorous solution. However, an adequate excitation of the radiating element can be achieved by properly designing a matched feed structure. In principle, the feed network with minimized reflections can be achieved by using properly designed transitions.

3.1 Slotline transitions

Various transitions for feeding the endfire slotline antennas are shown in Figure 7; these are

- microstrip or stripline-to-slotline,

- finline-to-slotline,

- coplanar waveguide(CPW)-to-slotline,

- microstrip-to-balanced line-to-antipodal slotline,

- uniplanar microstrip-to-slotline,

- uniplanar microstrip-to-coplanar waveguide(CPW).

15
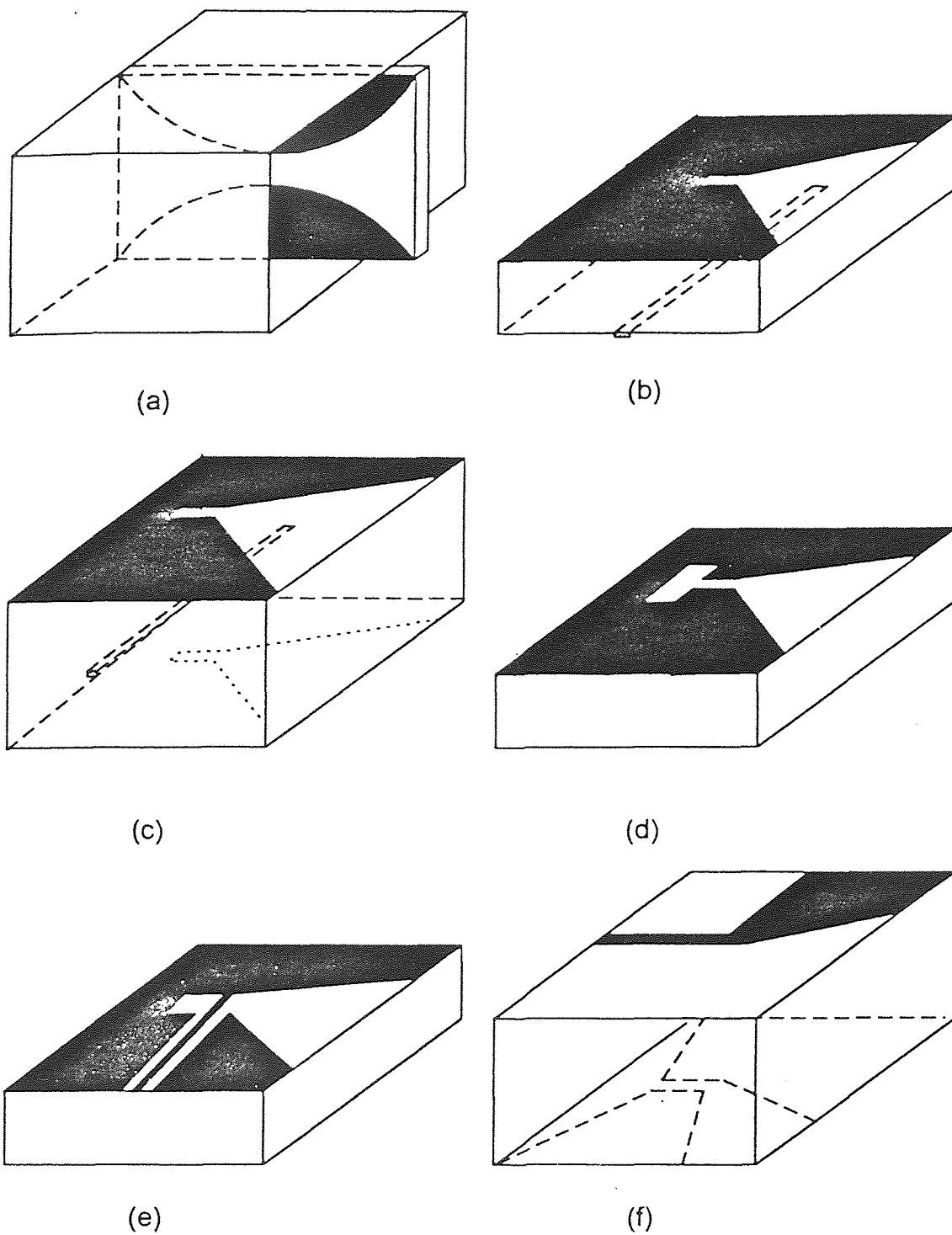
Figure 7. Types of transitions for tapered slot antennas. (a) finline-to-TSA ;
(b) microstrip-to-TSA; (c) stripline-to-TSA; (d) slotline-to-TSA ;
(e) coplanar waveguide(CPW)-to-TSA; (f) microstrip-to-balanced
line-to-antipodal TSA.

The most commonly used transitions in the microwaves frequencies are the stripline and microstrip-to-slotline transitions. The microstripline transition is especially suitable for systems in where the antenna is integrated with MMIC units, and built using the same technology. However, the stripline transition is more compatible with corporate feeds commonly used in phased arrays.

There are several advantages to using the stripline transition over the microstripline transition, such as:

- the symmetry of the feeding structure, between the dual slotline and the central stripline, may improve the radiation characteristics of the antenna (Figure 7(c)),

- the metallic enclosure of the stripline prevents radiation from the feed and undesirable coupling with the antenna.

- the feed transition is easier to match than the microstrip-to-slotline transition. This is confirmed by modeling the stripline transition with two microstrip transitions in parallel and thereby observing that the design of the slotline involves a double impedance value; this provides the designer more freedom from the physical limitations of the etching process.

Operation of these transitions is based on electromagnetic coupling, which is induced strongly in the microstrip-to-slotline transition region when quarter wavelength sections from the slotline and the microstrip cross each other (see Figure 8(a)).

The quarter-wavelengths sections function in the transition zone (the intersection of the two lines) as
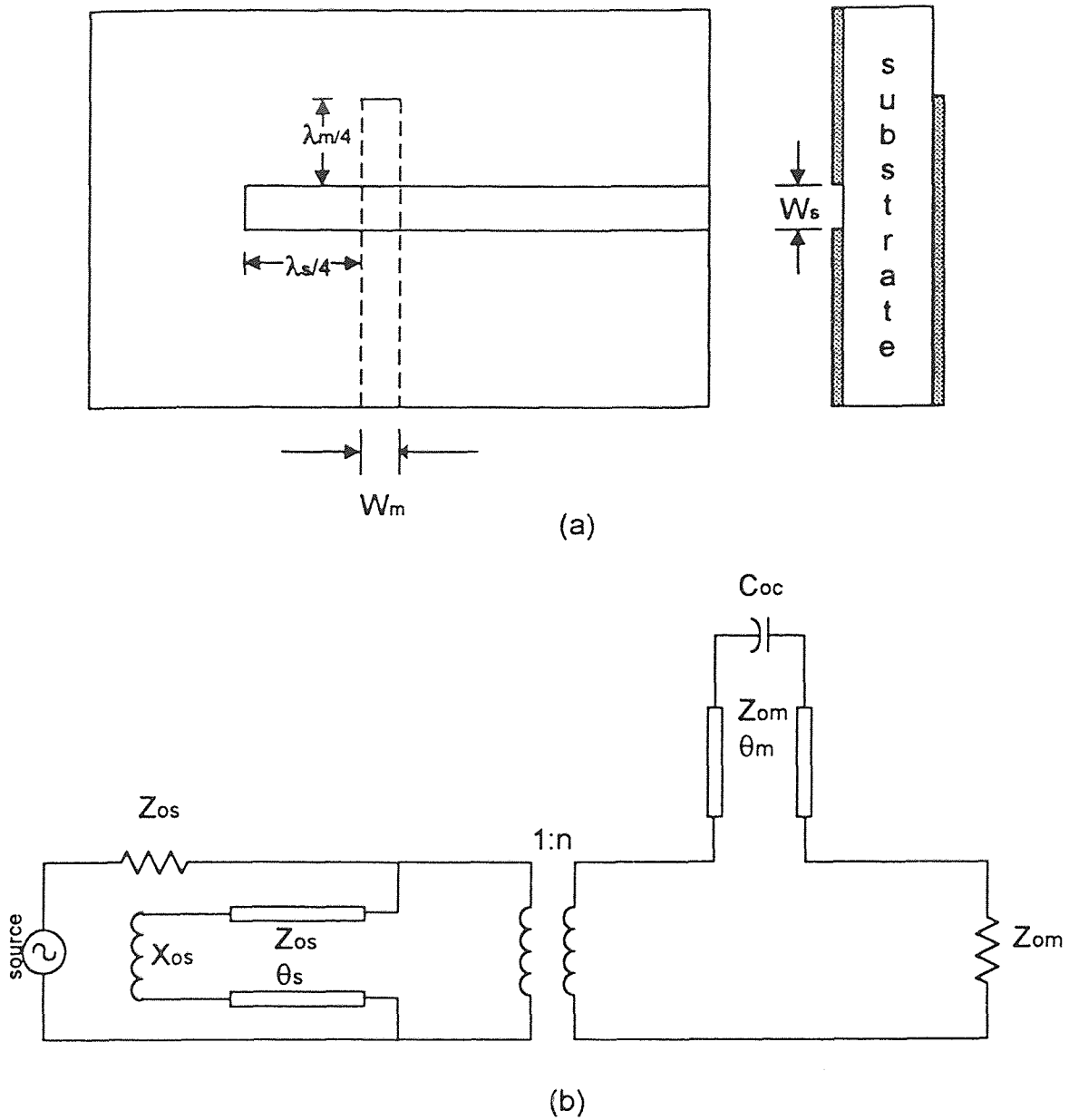
Figure 8. Microstrip-to-slotline transition. (a) Top and cross-sectional views (solid line = slotline trace, dashed lines = microstrip trace); (b) Knorr's equivalent circuit model.

- a short-circuit produced by the $\lambda/4$ transformation from the open circuit in the microstripline eliminates the perpendicular E-field in the strip;

- an open circuit on the slotline produced by the $\lambda/4$ transformation of the short circuit in the slotline reinforces the tangential component of the E-field, which is identified witn the residual field of the microstripline.

In summary, in the cross junction, the E-field changes from being perpendicular to the substrate plane in the microstripline to being tangential to the slotline.

A simple equivalent circuit for the microstripline-to-slotline transition was developed by Knorr[12] (see Figure 8(b)), where usage of formulae for the slotline parameters in [13] and laboratory measurements produced a good match in an octave range of frequencies (2 - 4 GHz).

The same lengths of the structure, i.e., quarter-wavelength uniform lines imply a narrowband behavior. This encouraged many researchers to investigate different configurations (nonuniform transmission lines) to reduce the narrowband limitation of the uniform transitions that would reduce the overall performance of a wideband antenna .

In Figure 9 there are examples of wideband transitions. Figure 9(a) shows a transition designed by Robinson [14] in which a mechanism similar to the microstripline-to-slotline transition, but with a slightly different geometry, is used. In this case, the open circuit quarter-wavelength is a radial stub, and the quarter-wavelengths uniform sections are a 50 ohms microstripline and 72 ohms slotline.The VSWR obtained was less than 1.1 for 8 to 10 Ghz (20 % bandwidth) The following three cases (Figures 9(b),(c) and (d)) are also wideband transitions, but with the strip shorted to the ground plane. The transition with a
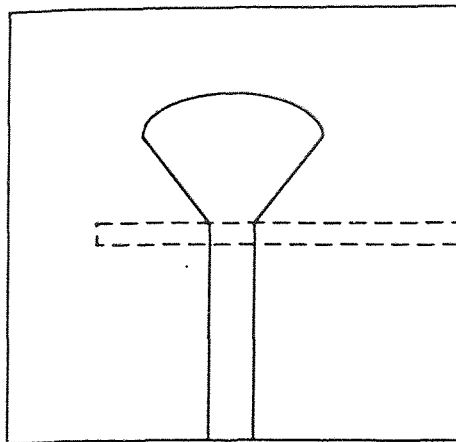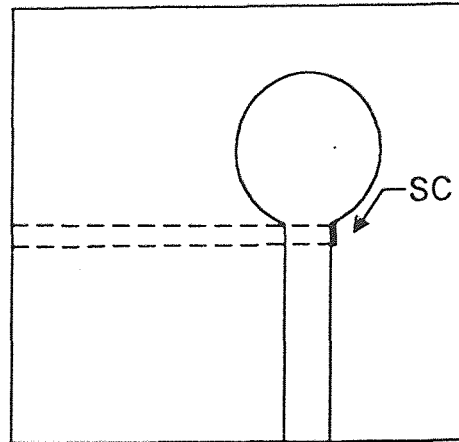
SC = short circuit
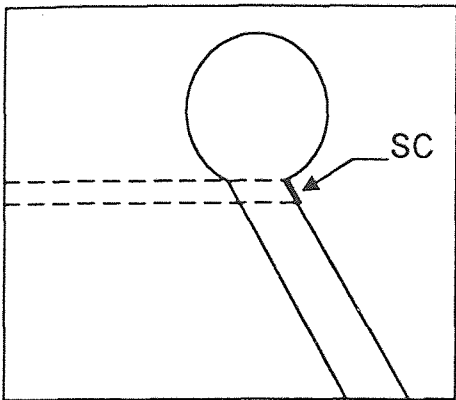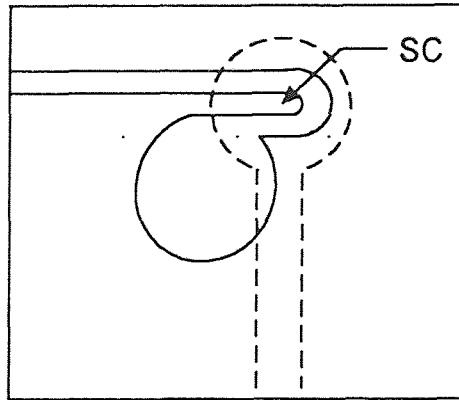
Figure 9. Wideband microstrip-slotline transitions (solid lines = slotline trace, dashed lines = microstrip trace). (a) grounded radial slotline stub; (b) Circular slotline stub with grounded microstrip; (c) Circular slotline stub with tappered grounded microstrip; (d) Spiral slotline with grounded circular microstrip.

spiral shape[15] produced a VSWR less than 1.1 in the 1 to 10 GHz frequency range. Another broadband transition from 1 to 10 GHz with an insertion loss less than 0.2 dB was reported in [16], but a different principle was used (6-port junction). Schuppert [17, 18], presented a systematic study of microstripline to slotline transitions. His analysis was based on a network description through transmission-line models and was verified experimentally. The different transitions studied by Schuppert are illustrated in Figure 10 and the transmission-line model used is shown in Figure 11. Measured results confirmed experimentally that nonuniform transitions have a wider bandwidth than the uniform lines.

One of the first theoretical studies with a more rigorous approach representing the transition by a transmission-line model was developed by Yang [19]. This study resulted in a dynamic model that took into account all the physical effects, such as, the radiation and surface waves due to the cross-junction, line discontinuities, and all the mutual coupling due to the dominant mode as well as higher order modes of each line.

So far, most of the research and development has been directed toward improving the wideband behaviour of the microstrip to slotline transition or similar multiplanar transitions. An example of uniplanar transition is the coplanar waveguide to slotline transition; its main advantage is that both slotline and coplanar waveguide can be printed in the same plane, discarding the need of via holes for ground connections or the precise location of the quarter wavelengths for electromagnetic coupling. It was reported that the uniplanar transition[20] has a total insertion loss of about 0.35 dB over a 5:1 bandwidth(2 - 12 Ghz). In antenna applications, this transition is valuable for integration of wideband LTSAs excited by a balanced arm feed printed on the same plane as the antenna.
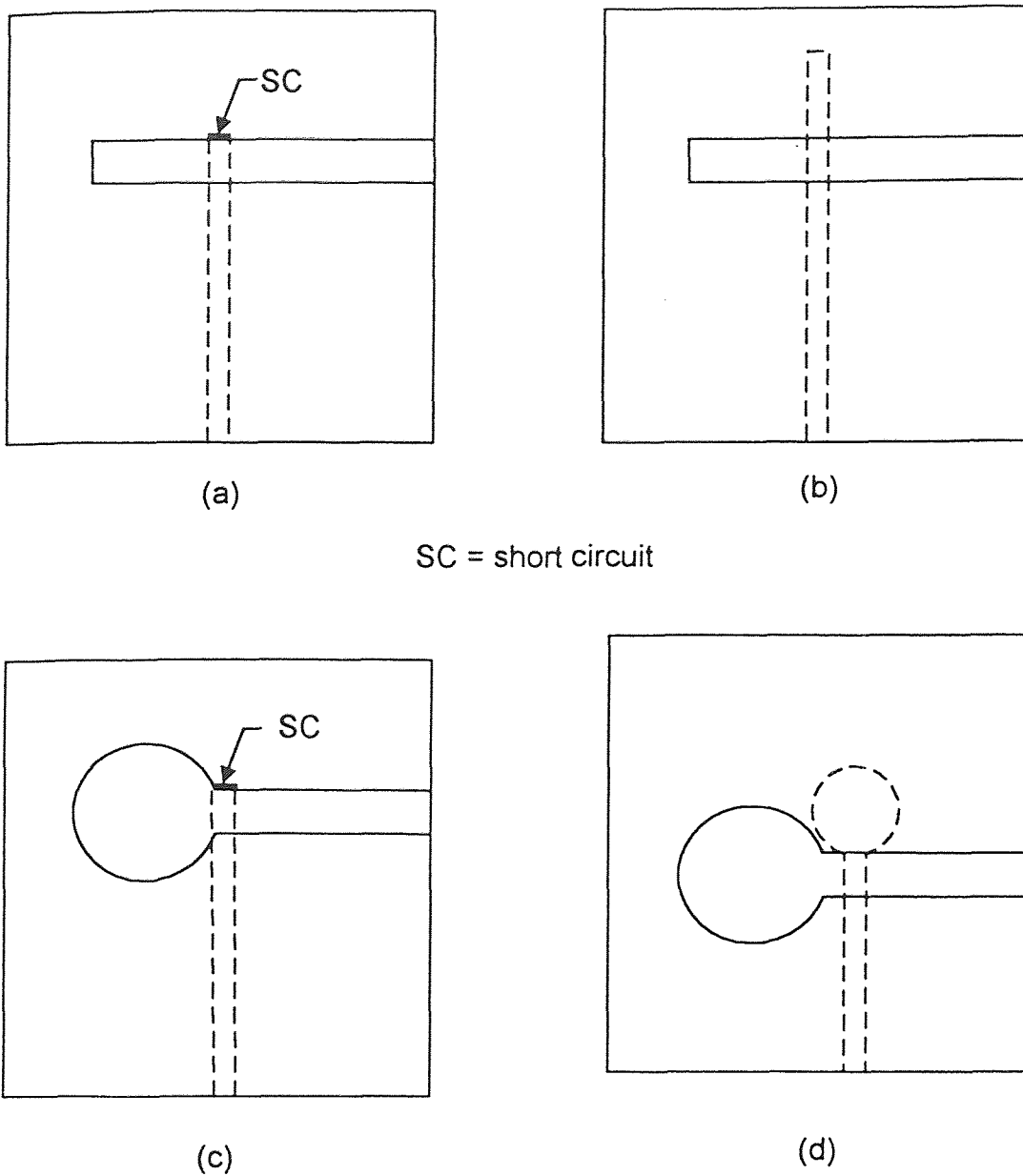
Figure 10. Microstrip-to-slotline transitions [15] (solid lines = slotline trace, dashed lines = microstrip trace). (a) grounded microstrip and λ/4 uniform slotline; (b) uniform λ/4 slotline and uniform λ/4 microstrip; (c) grounded microstrip and nonuniform circular slotline stub; (d) Nonuniform circular slotline stub with nonuniform circular microstripline stub.
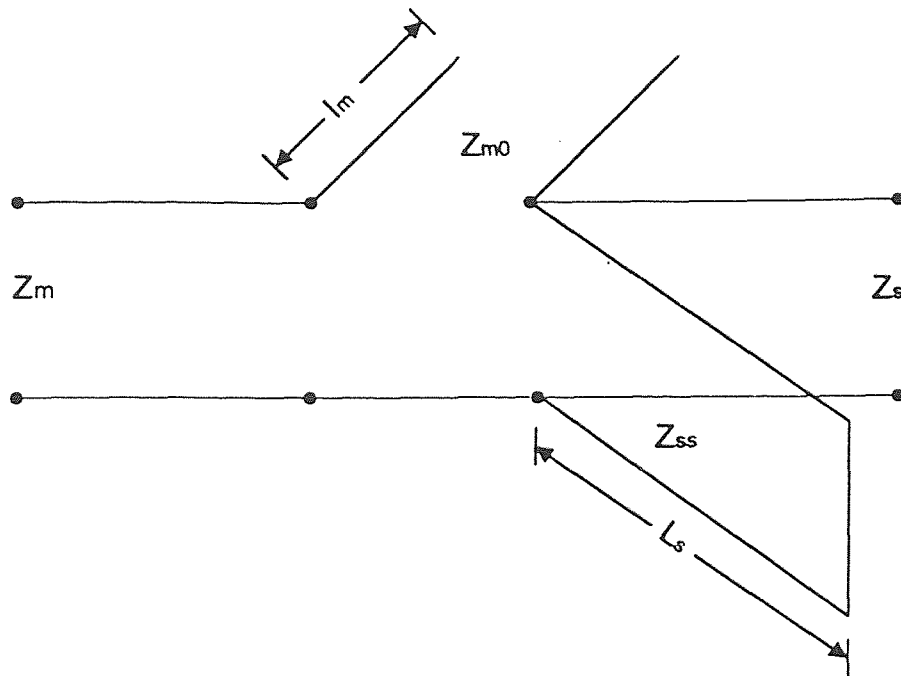
Zmo = characteristic impedance of the open microstripline
Zss = characteristic impedance of the shorted slotline
Zm = characteristic impedance of the microstripline
Zs = characteristic impedance of the slotline
Lm = length of the open microstripline
Ls = length of the shorted slotline.

Figure 11. Simplified transmission line model of a microstrip-to-slotline transition
used in [15]

3.2 Tapered Slot Antennas

The tapered slot antenna (TSA) is an endfire planar radiator that consists of a tapered slot, which is etched in the metalization on a thin and low-dielectric microwave substrate, and a transition from the feed line (stripline, microstripline, finline, etc.) to the slot antenna.(see Figure 7(a), (b), (c), (d)).

Applications of tapered slot antennas date back to the late 1950's. In a paper presented by Stephenson et.al., [21] the flared-slot antenna was introduced. This flared-slot antenna, an antecedent to the TSAs, consisted of a dielectric-filled waveguide that ended in a tapered-depth flared slot aperture (see Figure 12). Later, Eberle et.al. [22] developed the flared slot design for aircraft applications, highlighting the convenient integrability of its flush shape to the aircrafts's shape.

In 1979, Gibson [23] presented his pioneering paper on the "Vivaldi" antenna. His antenna consisted of a stripline-fed exponentially tapered slot that was etched out from a metalized Alumina substrate in a 8-40 GHz video receiver module. This was the first planar antenna which presented a symmetric E- and H-plane beamwidth, low sidelobes, and moderate gain over a very wide bandwidth(3:1 bandwidth).

The attractive features of tapered slot antennas are

- broadband operation,

- ease of integration of their planar structure to the MMIC and millimeter-
wave technologies,

- narrower beamwidths than the broadside antennas(excepting the log-
periodic and spiral antennas),
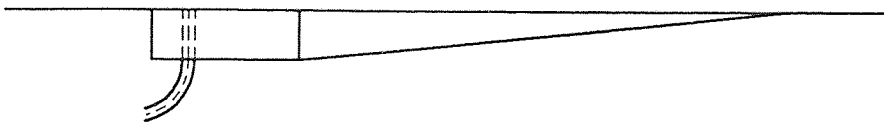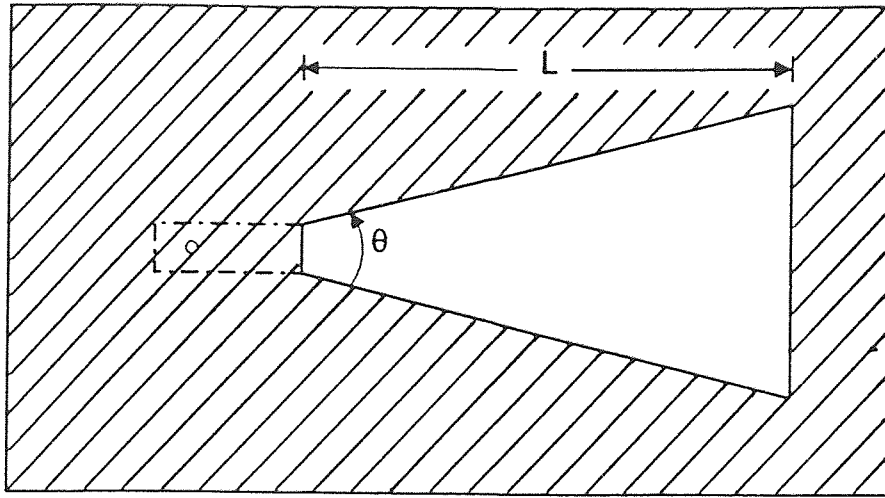
Figure 12. Flared-slot antenna

- capability of producing closely packed arrays , which outweigh the poor beam efficiency intrinsic to their open structure.

Different varieties of TSAs, which are mostly defined by the shape of the taper, are explained below (Figure 13).

3.2.1 Linearly Tapered Slot Antenna (LTSA) with air as a dielectric

The long wire antenna (antenna length $L > \lambda_0/2$) is one of the simplest traveling-wave wire antennas. This antenna has a radiation pattern with the main beam located at an angle of about 15 to 20 degrees off the endfire direction when its length is larger than a few wavelengths [24]. Since the current on the LTSA is mainly concentrated near the edge of the taper, an elementary model of a LTSA consists of two long wire antennas separated by an angle 2θ. The actual beamwidth of the LTSA and the one obtained from this model do not match [25]. An improved model is obtained by modifying the fin-antenna shown in Figure 14, so that it resembles the TSA. Carrel [26] analyzed the infinite finline using conformal mapping to find the impedance and field distribution; his results agreed more closely with experimental data [27]. Ingvesson et.al. [25] found that the beamwidth of LTSAs with air as a dielectric follow the $\sqrt{\lambda/L}$ dependence, which is characteristic of traveling-wave antennas [9]. This LTSA with air as a dielectric is a useful antenna but the ratio $c/v_{ph} \approx 1$ precludes it from obtaining the optimum gain.

3.2.2 Linearly Tapered Slot Antenna (LTSA) with a dielectric substrate

The general theory of traveling-wave antennas assures that there exists an optimum amount of dielectric for which the ratio c/v_{ph} , in this case in the LTSA, produces the optimum gain. Taking this into account and with the Zucker's design principles for surface-wave antennas [9], Ingvesson et.al. [27] deduced from experimental data that antennas with thin substrates and low dielectric constants were well-behaved
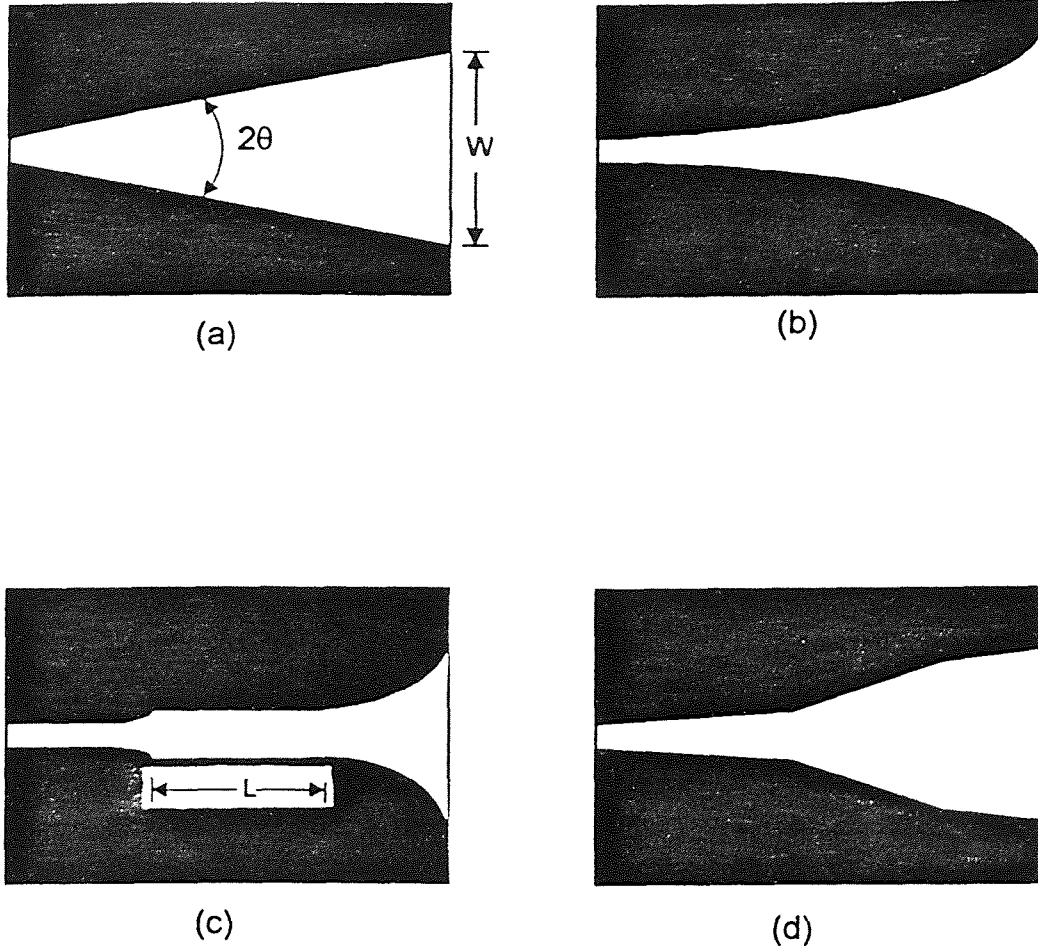
Figure 13. Tapered slot antennas.(a) Linearly Tapered Slot Antena (LTSA);
(b)Vivaldi antenna; (c) Constant Width Slot Antenna (CWSA);
(d) Broken Linearly Slot Tapered Antenna (BLSTA).
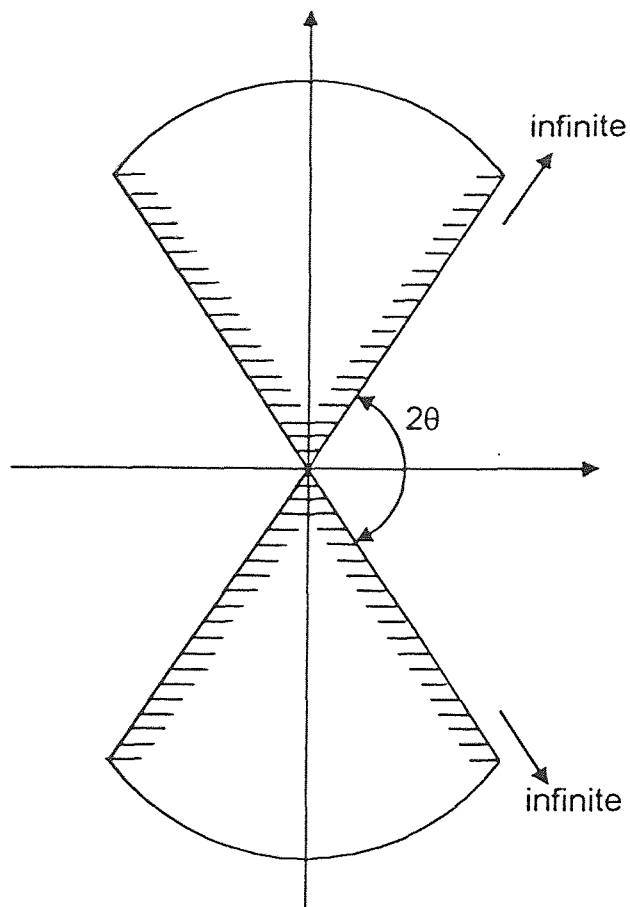
(a)
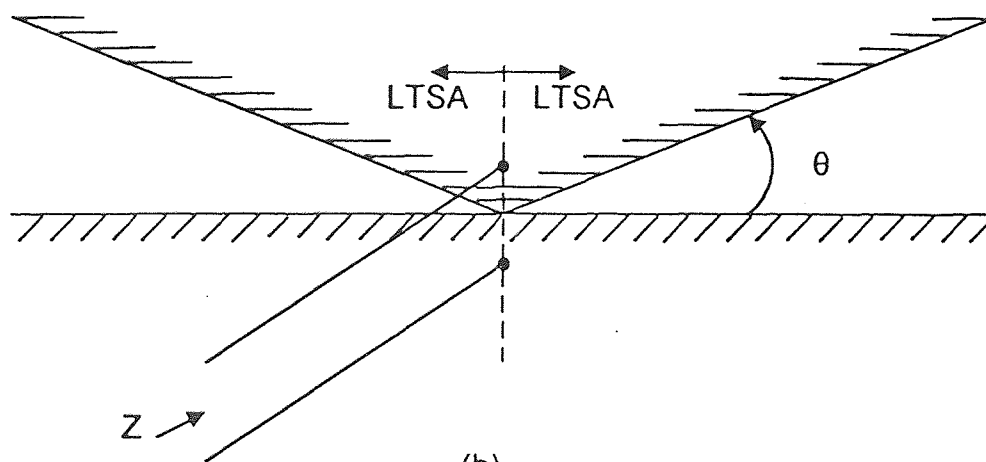
(b)

Figure 14. Fin antenna and double LTSA. (a) infinite fin-antenna studied by Carrel [24]; (b) mirrored double LTSA in a ground plane for impedance measurement.

traveling-wave antennas. As a result of this study, a very important design parameter was defined, namely, the effective dielectric thickness t_{eff},

$$t_{eff}/\lambda_0 = (\sqrt{\varepsilon_r} - 1)(t/\lambda_0) \tag{11}$$

where t is the actual substrate thickness. From [27], it was also found that for optimum performance, t_{eff}/λ_0 must satisfy the following relationship for antenna lengths from $3\lambda_0$ to $10 \lambda_0$:

$$0.005 < t_{eff}/\lambda_0 < 0.03 \tag{12}$$

For thicker substrates, a LTSA antenna will not display travelling-wave antenna characteristics.

Another important parameter to consider is the cutoff wavelength; it is defined as

$$\lambda_c = 2w \tag{13}$$

where w is the aperture size of the TSA (Figure 13). The importance of this parameter comes from the fact that if w is less than $\lambda_0/2$, the antenna no longer behave as a broad-band traveling-wave antenna. The first LTSA reported was the design made by Prasad and Mahapatra [28]. Their antenna was not an efficient one because its length ($L \approx \lambda_0$), and aperture (about $\lambda_0/4$) did not comply with the requirements for being an optimum endfire traveling-wave antenna, i.e., did not satisfy (12) and (13). Once t_{eff} and λ_c are considered, a set of rules [27] for designing these antennas can be used (Table.1)

Table 1 Basic formulae for the design of endfire traveling-wave antennas

	Maximum gain	Low sidelobes/ broad bandwidth
Directivity (dB)	$10 \log(10L/\lambda_o)$	$10 \log(4L/\lambda_o)$
Beamwidth (degrees)	$55/\sqrt{L/\lambda_o}$	$77/\sqrt{L/\lambda_o}$
Optimum velocity ratio (Hansen-Woodyard)	$c/v_{ph} = 1 + 1/(2 L/\lambda_o)$	

3.2.3 Vivaldi antennas

The Vivaldi antenna can be designed with a multi-octave bandwidth and a constant beamwidth for more than one octave [23]. The low frequency range of this antenna is limited by the aperture of the antenna (w), and must comply with condition (13). At high frequencies the thickness t will limit its performance when (13) is no longer applicable.

The opening angle 2θ has a very large effect on the performance of this antenna, contrary to what was observed for the LTSA in [27]. The shape contour of the Vivaldi antenna is typically defined by

$$y = \pm A\exp(px) \tag{14}$$

As frequency varies, different parts of the antenna radiate while the size of the radiating part remains constant. Theoretically, therefore, a Vivaldi antenna with a long length has an unlimited operating frequency range, over which the beamwidth remains constant. Typical radiation patterns of a Vivaldi antenna are shown in Figure 15 [27]. The triangular pattern shape is typical of gradually curved, slow-wave Vivaldi antennas.
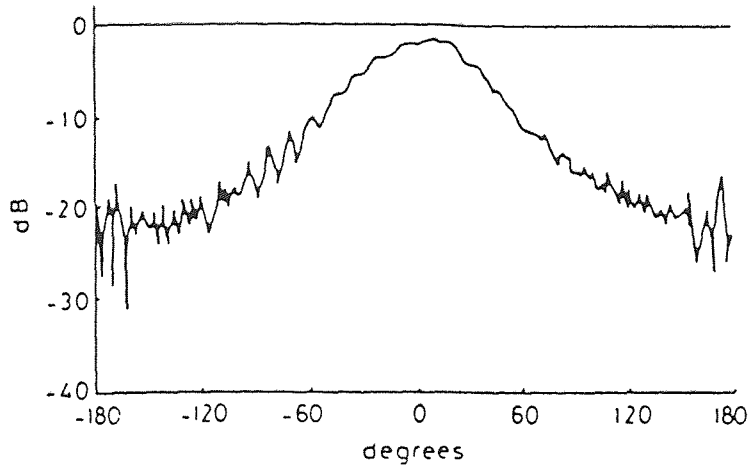
(a) E - plane
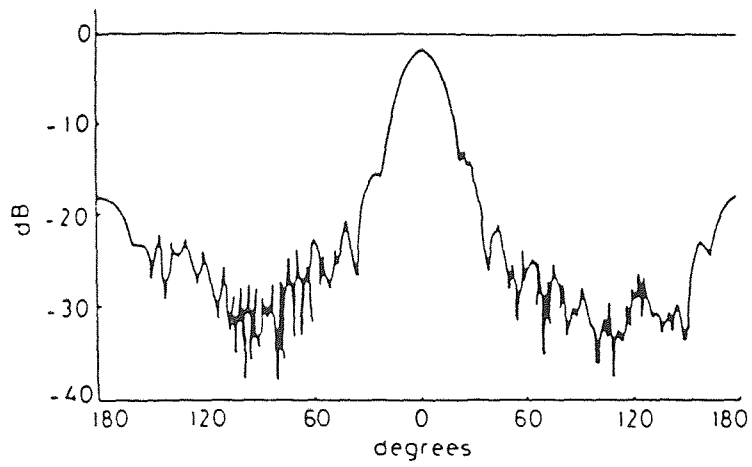
(b) H - plane

Figure 15. Radiation patterns of a Vivaldi antenna.

3.2.4 Constant Width Slot Antenna (CWSA)

This antenna consists of a slot of constant width and has a better packing density in focal plane imaging arrays [29]. An efficient CWSA consists of a exponential taper from a narrow slot to a $0.8\lambda_0$ constant width slot and a maximum length between $4\lambda_0$, and $5\lambda_0$.

3.2.5 Broken Linearly Tapered Slot Antenna (BLTSA)

The BLTSA is an alternative antenna design to reduce the high cross-polarization levels in the diagonal plane (D plane) that is inherent in the TSAs (LTSA,CWSA). This antenna consists of three sections (Figure 13(d)) and yields a lower (approximately 2dB) cross-polarization ratio in the D plane than the LTSA and the CWSA[30]. This is due to the shorter distance between phase centers of the E- and H-planes. The BLTSA requires a smaller dielectric supporting structure, which is advantageous when working at millimeter-wave frequencies.

CHAPTER 4

FINITE-ELEMENT METHOD

Various numerical techniques are applicable to model radiation from tapered slot antennas. Because of the physical dimensions of these structures and available computational packages, the finite element method was chosen for CAD of linear tapered slot antennas.

4.1 Foundations

The finite element method is an approximate numerical procedure to find solutions to a boundary-value problems. This method was first proposed by Courant [31] in 1943. Initial applications in 1950s were restricted to aircraft design. Since then, there has been a considerable concentration of research and development to refine the method for use in the area of structural design. It was not until late 1960s that interest in this numerical method for electromagnetic (EM) problems started to appear, examples of diverse applications include waveguide problems, electric-machinery related problems, semiconductor devices, microstriplines, and many more.

Basically, the form in which this method is implemented starts by replacing the continuous problem region by subregions (finite element) in which the unknown function is defined by interpolation functions with coefficients to be determined. Then, by applying the Ritz variational principle or the Galerkin procedure, a certain number of algebraic

expressions is obtained, and finally the boundary-value problem is solved by determining the coefficients of the approximate algebraic system.

In solving boundary-value problems, the finite element method involves the following steps:

- Mesh generation,

- Determination of the interpolation functions,

- Establishment of the algebraic system,

- Solution of the algebraic system,

- Mesh generation

The subdivision of the region of interest is the first step in any finite element analysis. This division influences the computer memory capacity, the computation time and, indirectly, the accuracy of the results. The subdivision of the problem region yields a number of subregions or finite elements. In one-dimensional analysis, these domains consist of straight or curved lines, elements in terms of short line segments that joint together to form the original line (Figure 16(a)). In the 2-dimensional case, the elements are normally triangles or rectangles (Figure 16(b)). The rectangular ones are adequate for rectangular regions, while the triangular ones are used for irregular regions. In the case of a 3-dimensional region, it may be subdivided into tetrahedras, triangular prisms, or parallelepipeds (Figure 16(c)); among these the tetrahedra is the simplest and most suitable element for representation of an arbitrary-volume domain.

The linear line segments, triangles and tetrahedras are the basic finite elements in their respective domain (dimensions) and can model curved lines or surfaces by
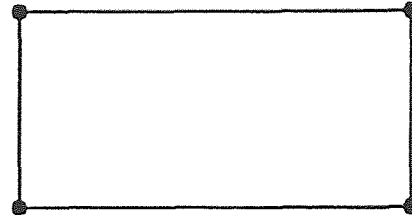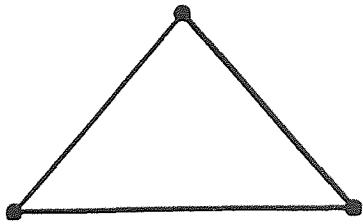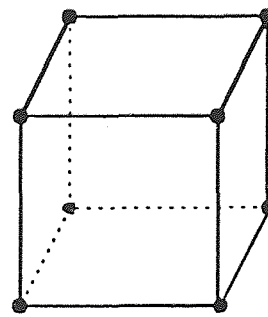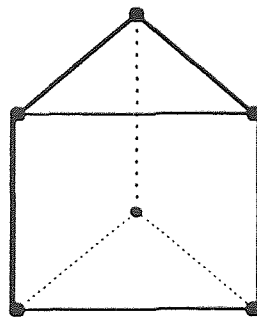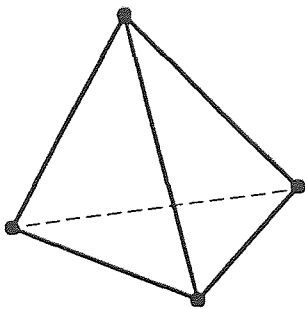
Figure 16. Basic finite elements.(a) 1-D ; (b) 2-D ; (c) 3-D.

straight line segments or planar patches. In Figure 17 an example of discretization of a 3-D region of a tapered slot antenna is depicted.

Normally, a finite element solution is based on assuming unknown functions φ at each node of an element. Part of the solution of the problem requires the description of the nodes by its coordinate values, local number and global number. The local number of a node provides information about its position in the element, whereas the global number specifies its position in the whole system. The local and global characterizations of the nodes must be dealt with carefully. Solutions using the method produce banded matrices whose bandwidths are determined by the maximum difference between the global numbers of two nodes in an element. This gives us some insight into how to minimize computer processing cost, that is, the strategy on the numbering of these nodes must be adjusted in order to minimize the bandwidth.

- **Selection of the interpolation functions**

An interpolation function is selected to provide an approximation of the solution inside the element. Polynomials of first (linear), second (quadratic), or higher order are usually used.

The linear interpolation is preferred because higher order polynomials require more complicated formulation. For the chosen order of the polynomial, the unknown solution in an element is expressed in the following form:

$$\phi^e = \sum_{j=1}^{n} N_j^e \phi_j^e = \{ \phi^e \}^T \{ N^e \} \tag{15}$$

where n is number of nodes in the element, ϕ_j^e is value of ϕ at node j of the element, and N_j^e is the basis function with nonzero value only inside the element.
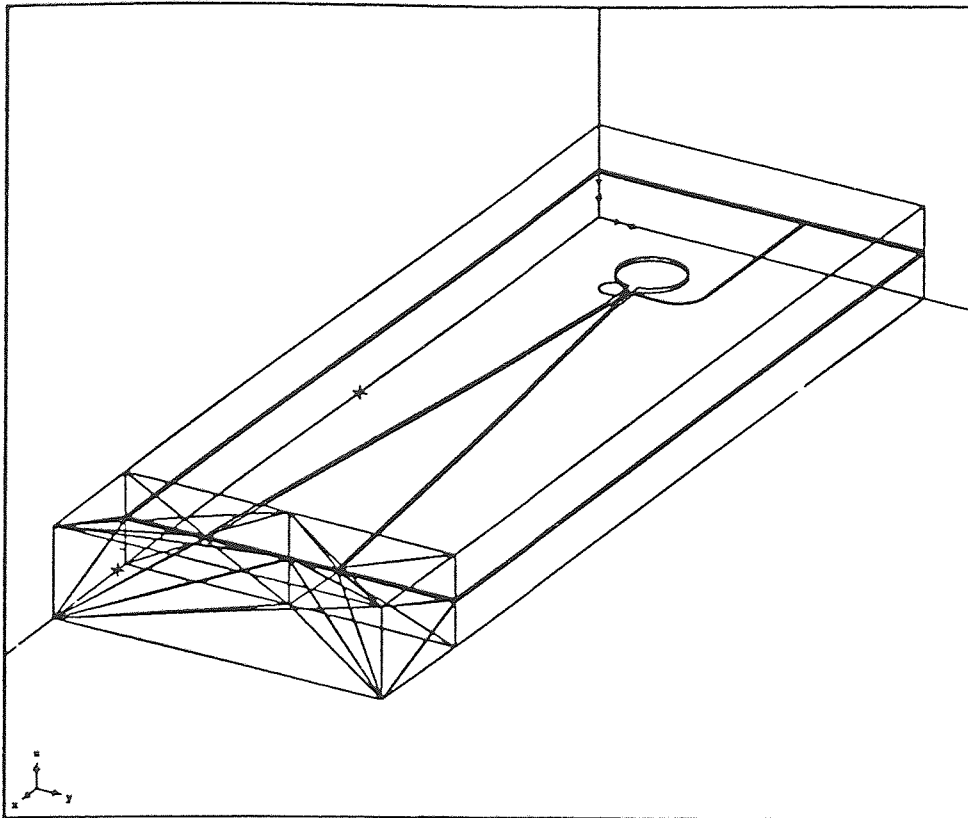
Figure 17. Finite element 3-D meshing of a part of a LTSA model.

- Formulation of the system of equations

The Ritz variational and Galerkin methods are usually used to form system of equations. Using either method, an elemental equation is formed. Then, all the elemental equations are summed over all the elements to form a system of equations. Finally, the boundary conditions are applied to get the final system of equations.

- Solution of the system of equations

The system of equations formed has one of the forms:

$$[K]\{\varphi\} = \{b\} \tag{16}$$

or

$$[A]\{\varphi\} = \lambda[B]\{\varphi\} \tag{17}$$

The first equation (16) is derived from either an inhomogeneous differential equation or inhomogeneous boundary conditions or both. This is an equation system of deterministic type that is associated with the radiation and scattering phenomena in the presence of a source or excitation.

Equation system(17) is associated with homogeneous differential equation and homogeneous boundary conditions. This equation system is referred to as an eigenvalue type and is associated with source-free problems, such, as wave propagation in waveguides and resonances in cavities. After solving the system of equations for $\{\varphi\}$, required parameters such as current distribution, impedances, radiation patterns, etc., are determined.

4.2 High Frequency Structure Simulator (HFSS).

The High Frequency Structure Simulator (HFSS) marketed by Hewlett-Packard Company is based on the finite element method to solve the full-wave equations for fields.

The typical steps in HFSS analysis are

- Mesh generation

HFSS applies the Delaunay tessellation which is based on the concept that an optimal triangular mesh is one in which no triangle circumcircled contains any other triangle vertex in its interior. This method is extended to 3-D [32] by using a similar relationship between the tetrahedrons and the corresponding circumspheres.

- Interpolation functions

For practical reasons quadratic polynomials are used.

- Formulation and solution of the equations systems

The simulator uses for these two steps the transfinite element method. In the 2-D case, this method consists of using one-dimensional analytical solutions in the port regions as basis functions within a variational framework to approximate the fields in the ports. This method is extended to 3-D problems, but since analytical solutions are not available in 2-D in general, these field solutions are obtained by using 2-D finite element analysis.

HFSS implemented these steps by creating the module "wave" (2-D port solver) and the module "mic3d" (3-D solver). The module "wave" determines the port excitations by computing the natural port characteristics: mode fields, propagation constants and impedances(see Figure 18). The module "mic3d" computes 3 types of S-parameters using the full-wave equation:

$$E(x,y)e^{jwt-\gamma z}$$ →

Wave module
$\nabla x((1/\mu)\nabla xE(x,y)) -$
$k_o^2 \varepsilon E(x,y) \qquad = 0$

→
$$\gamma = \alpha + j\beta$$
$$Z_{PI}, Z_{PV}, Z_{VI}$$
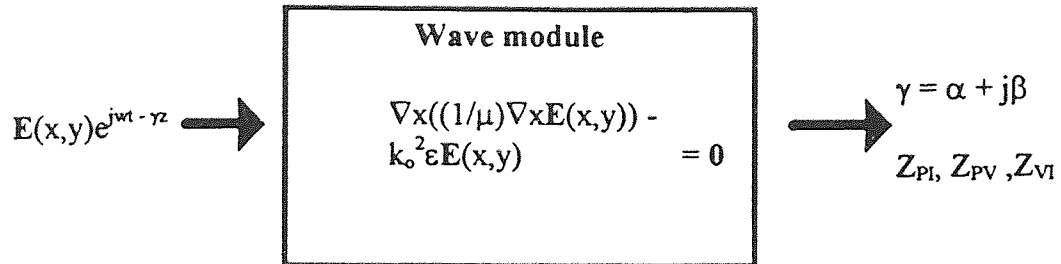
where E(x,y) is a phasor field quantity

      γ is the complex propagation constant $= \alpha + j\beta$

      α is the attenuation constant of the wave

      β is the phase constant associated with the wave

      w is the angular frequency, $2\pi f$

Z_{PI} is the impedance calculated from power (P) and current (I)

      $P = \int_S ExH^*.ds$

      $I = \int_C H.dl$

Z_{PV} is the impedance calculated from power (P) and voltage (V)

      $V = \int_C E.dl$

$Z_{VI} = \sqrt{Z_{PV} Z_{PI}}$

Figure 18. HFSS 2-D field solver: wave module.

- generalized S-parameters (all ports are matched),
- 50-ohm S-parameters,
- higher-order mode S-parameters(see Figure 19).

This simulator additionally includes some features that eliminate some intrinsic problems of the FEM, such as, the difficulty in the data entry and mesh generation and the presence of spurious modes. By solving these problems, HFSS lets the designer have full use of its main features, such as, flexibility in modeling complicated shapes and different materials, and efficiency in computational savings that comes from the sparse structure of the coefficient matrix.

$$E(x,y,z)e^{jwt} \quad \Longrightarrow$$

mic3d

$$\nabla \times ((1/\mu)\nabla \times E(x,y,z) -$$
$$k_o{}^2 \varepsilon E(x,y,z) \qquad = 0$$

$\Longrightarrow$ 50 ohms,
generalized, and
higher mode
S parameters:
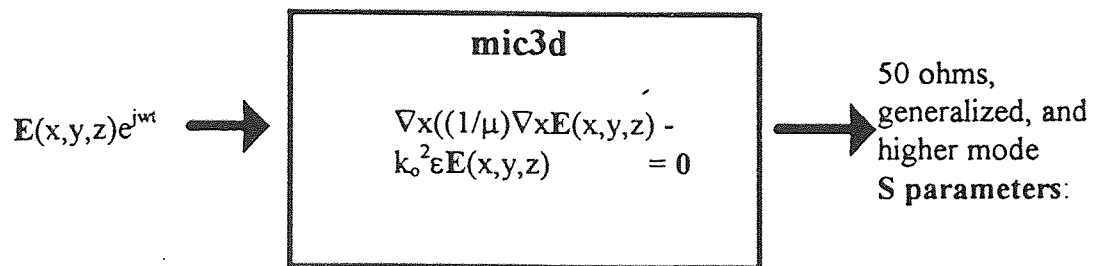
Where $E(x,y,z)$ is a 3-D phasor field quantity

k_o is the free space wavenumbe, $w\sqrt{\mu_0 \varepsilon_0}$

w is the angular frequency, $2\pi f$

$\mu(x,y)$ is the complex relative permeability

$\varepsilon(x,y)$ is the complex relative permittivity

Figure 19. HFSS 3-D field solver: mic3d module.

CHAPTER 5

CAD DESIGN OF A LTSA

The design procedure of a TSA is described below in two different configurations. One antenna is fabricated and experimental results are also presented.

5.1 Design Procedure

The design of a LTSA requires the following steps:

- Selection of the substrate material; the effective dielectric thickness t_{eff} of the material must be in the optimum range from 0.005 to 0.03 [27] to ensure that the antenna behaves as a surface-wave antenna,

- Design of the antenna; the parameter to consider is the aperture(w_{ant}), which must be greater than half a wavelength [27],

- Selection and design of the transition should be according to the specifications, e.g., if we require a wideband transition , a nonuniform transition must be chosen,

- Simulation and tuning of the antenna design requires optimization of various physical parameters until the desired response is obtained.

5.2 Stripline-fed LTSA

The operating frequency was chosen at 10 GHz and nonuniform stubs were utilized for the transition between the stripline feed and the two linearly tapered slot antennas that are placed at the bottom and top ground planes of the stripline (Figure 20).

The characteristics of the slotline were obtained by using the formula given in [33], and a corresponding computer program is included in Appendix A.

- Selection of the substrate material

LTSA requires low dielectric constant and a thin substrate material to yield the endfire traveling-wave characteristics [27]. The chosen substrate for these antennas in the X band consists of a double-sided metalized board with a dielectric constant ε_r =2.2 and a thickness d=10 mils. Substituting values of ε_r and thickness t data for t_{eff} in (11) results in t_{eff} =0.008, which is inside the desired optimum range (12).

The stripline structure (formed by joining two substrates of 10 mils thickness) leads to a stripline of height b=20 mils. Each side will have a LTSA, while the feed will be a stripline in between.

- Design of the antenna

The physical length of the LTSA has to be between 2 to 4 λ_0 and an aperture size w greater than $\lambda_0/2$. An aperture angle (2θ) in the range of 12^0 was considered in order for the antennas to have symmetrical E- and H-field beamwidths [27]. The following antenna parameters were chosen to comply with the above restrictions (see Figure 21):
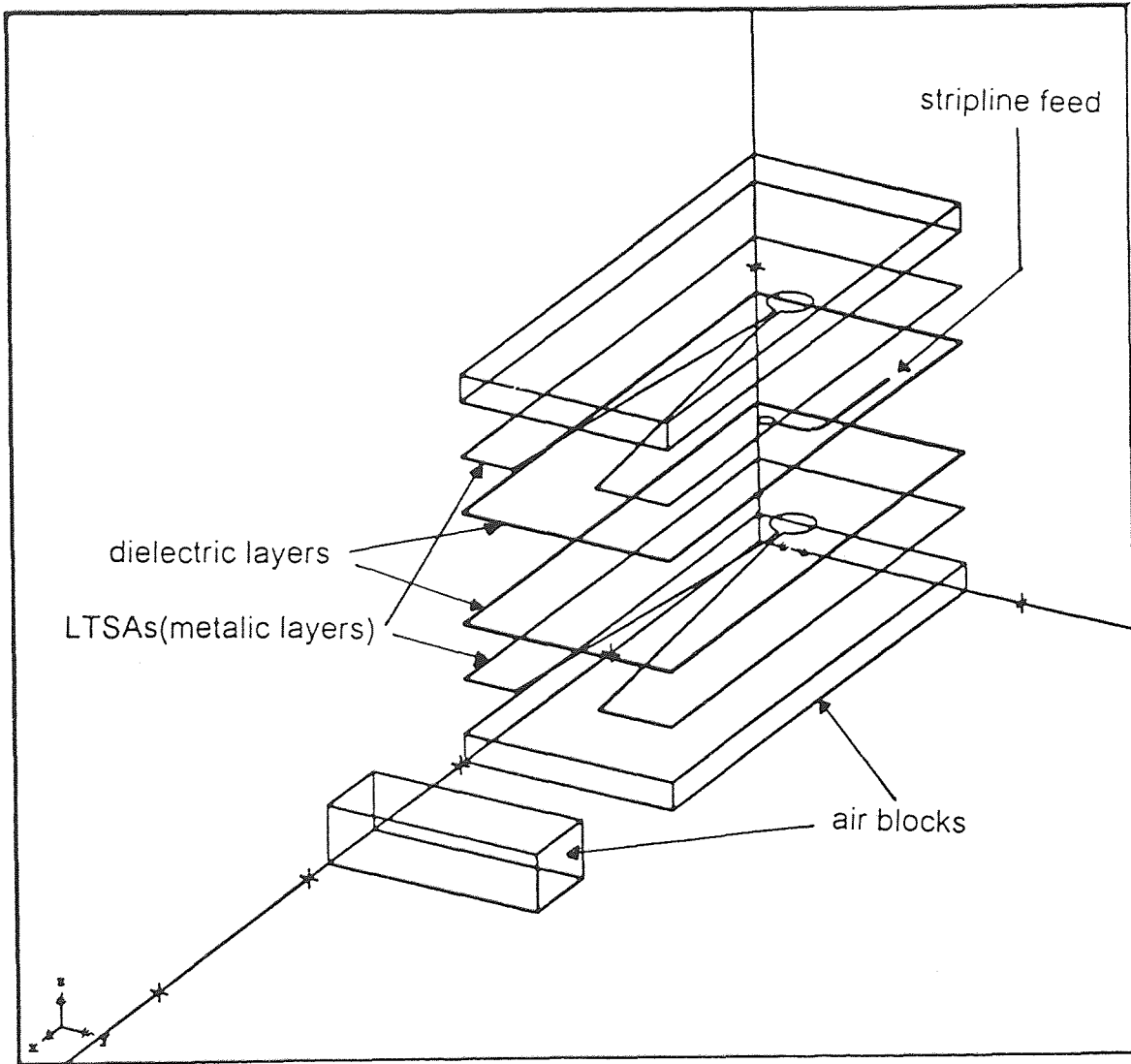
Figure 20. Geometrical objects of the stripline-fed LTSA model for HFSS simulation.
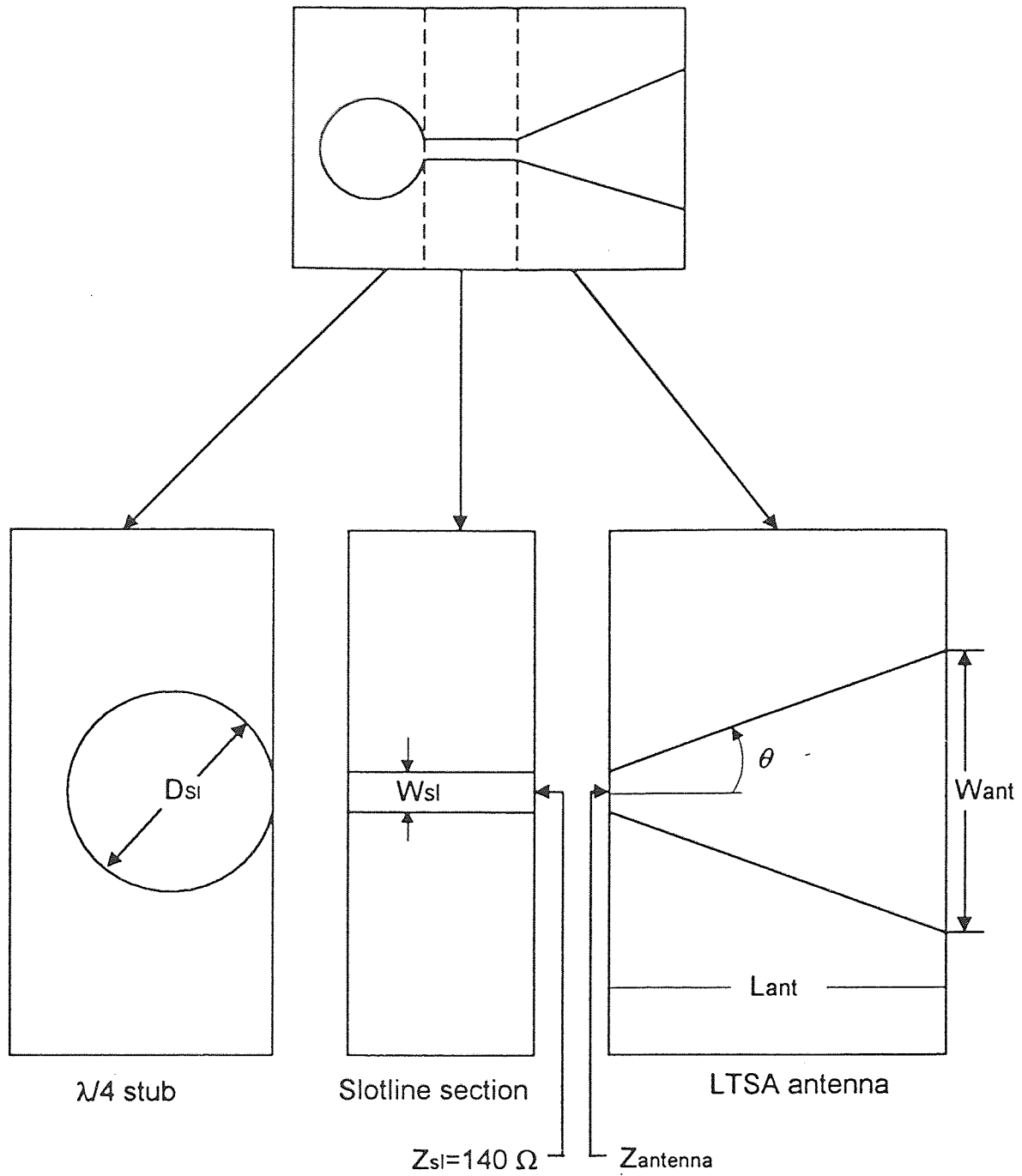
Figure 21. LTSA: wideband open circuit (λ/4) stub, slotline section and LTSA

$$L_{ant} = 2.4\, \lambda_0 = 2,834\ mils$$

$$2\theta = 12\ degrees$$

These values yield an antenna aperture size w_{ant} greater than $\lambda_0/2$ to operate as an endfire antenna (13)

$$w_{ant} = 2\, L_{ant}\, tg\theta + w_{sl} = 617\ mils > \lambda_0/2 = 590\ mils.$$

The value of 30 mils for w_{sl} is an assumed initial value in the design of the transition.

The antenna impedance of a LTSA varies in the range between 80 - 140 ohms [34], therefore, the characteristic impedance of the uniform slotline that joins the stub with the antenna (Figure 21) must be in the same range of values.

- Selection and Design of the transition

The widths of the uniform sections for the slotline and stripline are tabulated in Table 2. The initial values chosen in the design from Table 2, are $w_{sl}^{(0)} = 30$ mils and $W_{st}^{(0)} = 12$ mils. The initial value $w_{sl}^{(0)}$ was chosen to match the input impedance of the LTSA (140 ohms was taken as an initial value). To determine an initial value for $w_{st}^{(0)}$, the

Table 2 Physical dimensions of the uniform slotline and stripline transmission lines, where w_{sl} and w_{st} are the widths, Z_{sl} and Z_{st} are the impedances and λ_{sl} and λ_{st} are the wavelengths for the slotline and stripline, respectively.

SLOTLINE[1]			STRIPLINE[2]		
w_{sl}(mils)	Z_{sl}(ohms)	λ_{sl}	w_{st}(mils)	Z_{st}(ohms)	λ_{st}(mils)
40	150	$0.94\,\lambda_0$	12	60	796
30	140	$0.93\,\lambda_0$	17	50	796

1. Formulae for slotline characteristics for low dielectric were taken from [33] and a program is included in Appendix A.
2. Formulae for stripline characteristics were taken from [35].

simple model depicted in Figure 22 was used. The two identical slotlines in the transmission line model of the transition were replaced by a line with half the characteristic impedance of a slotline (due to the parallel configuration of the symmetrical slotlines). Thus, the two slotlines each of characteristic impedance 140 ohms were replaced by an equivalent slotline characteristic impedance of 70 ohms. Observing that the equivalent model for the stripline is similar to Knorr's model for the microstrip-to-slotline transition, one can assume that conditions for optimum match of the microstrip transition can be applied to this equivalent model.

The optimum match condition in a microstripline-to-slotline transition is reached when the characteristic impedance of the slotline is greater than the microstripline by 10-20 ohms [12]. Considering these design constraints, an initial value for $w_{st}^{(0)} = 60$ ohms is chosen for an optimum match. To realize the λ /4 stubs located in the transition, nonuniform transmission lines of circular shape were used. The initial diameter for the λ /4 slot stub was set equal to $D_{sl}^{(0)} = \lambda_0$ /4 , which is approximately equal to 300 mils at 10 Ghz. For the circular stripline λ /4 stub, an initial value for $D_{st}^{(0)} = \lambda_{st}$ /4 =200 mils was assumed, where λ_{st} is the wavelength in the stripline. This value was optimized with use of the circuit simulator MDS(Microwave Design System), in which the circular stripline stub was modeled by 40 equivalent sections of transmission lines (see Figure 23). The circuit simulation resulted in an initial value, $D_{st}^{(0)} = 120$ mils. The same procedure could not be applied to the analysis of the slotline short stub because the models of slotline in MSD do not accept a low value such as $\varepsilon_r = 2.2$.
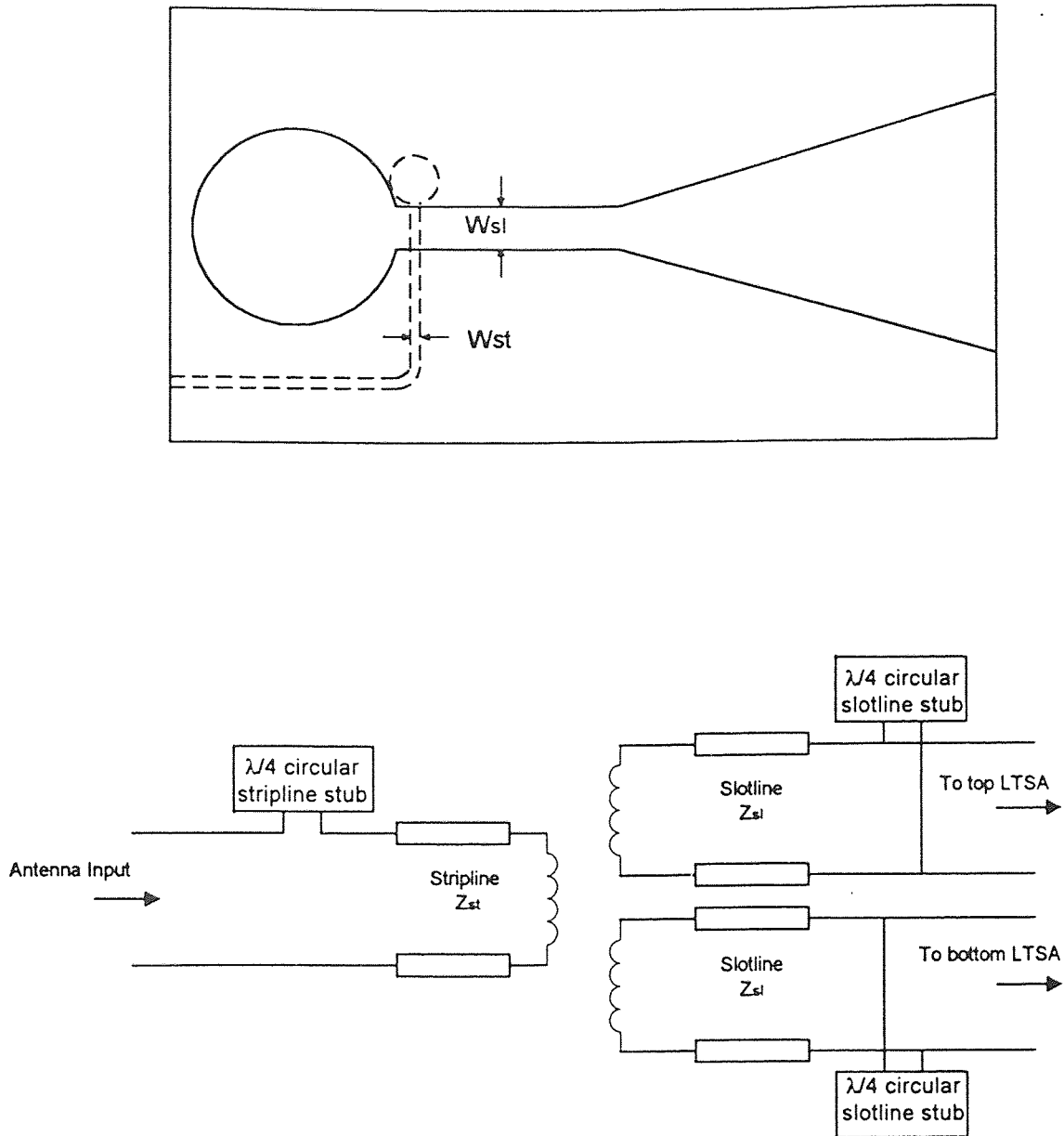
Figure 22.   Transmission line model for the transition of a stripline-fed LTSA
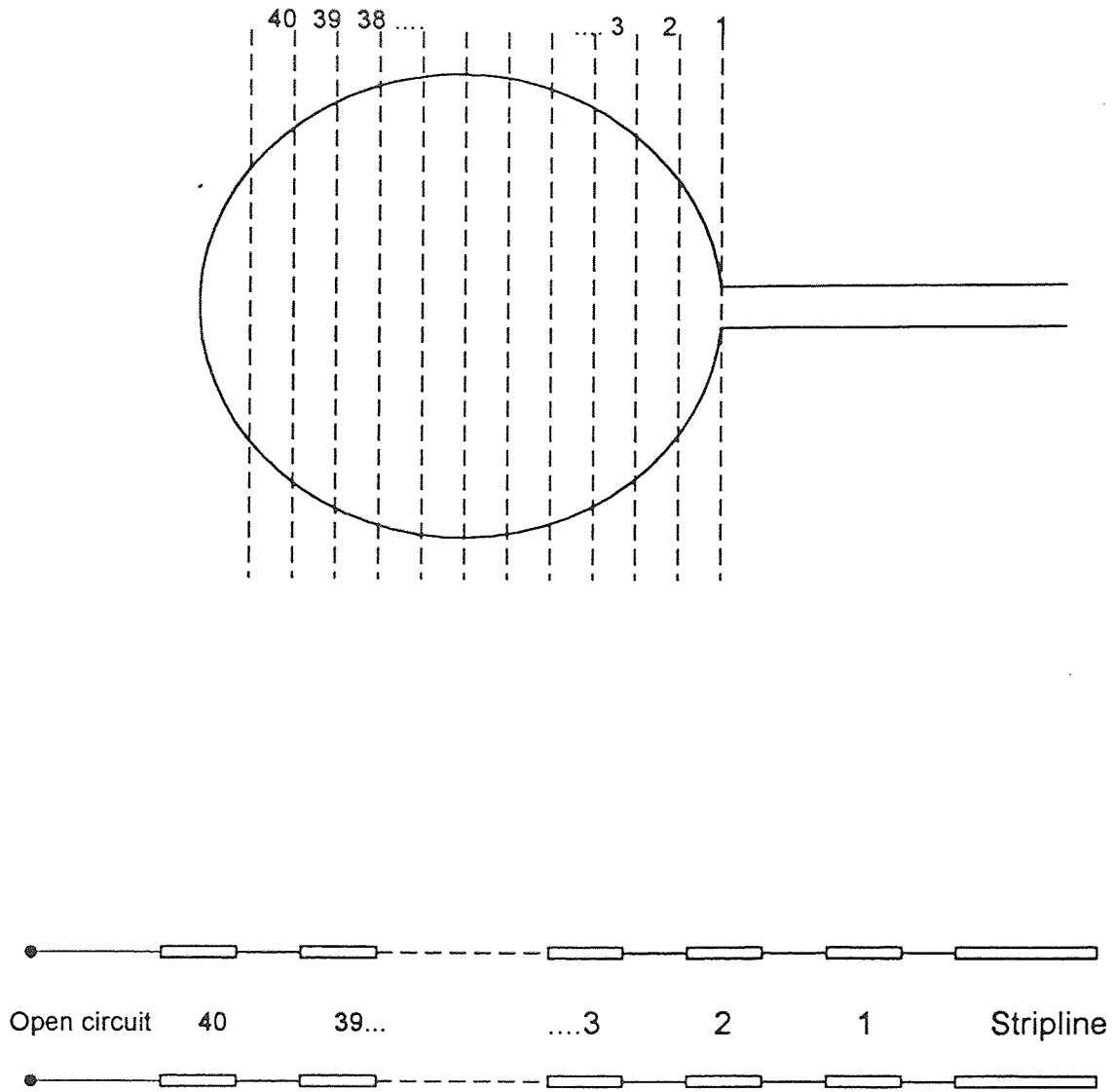
Figure 23. Transmission line model of a λ/4 circular stripline stub in a MDS simulator

- Simulation and tuning of the antenna

With the initial values outlined above, a finite element analysis was set-up using the HFSS

software code. The geometry of the problem was defined as consisting of two LTSAs, the

middle stripline feed and the dielectric substrate of the stripline (Figure 20). The boundary

conditions are adjusted according to a surface admittance of $Y_0 = 1/377$ mhos. The

operating frequency, the required accuracy and the number of iterations were determined;

in this case, the 80 Mbytes of dynamic RAM of the HP9000/715S was not adequate for

more than two iterations. The number of tetrahedra that resulted is approximately equal to

40,000, leading to a matrix of almost 100,000 elements. The goal of the simulation was set

to obtain a low value of $|S_{11}|$; for example, $|S_{11}| < 0.3$ is a reasonable goal since this implies

that approximately 10% of the energy is reflected to the feedline and the remaining 90% is

radiated. The results of the simulation for the initial estimates did not exhibit good

convergence. For that reason, the dimensions of the antenna were modified and tuned, i.e.,

the diameter D_{sl} of the circular slot stub and the slotline width w_{sl} , were varied. After a

number of trials an $|S_{11}|$ of around 0.3 was achieved with the following values:

$w_{sl}^{(f)}$=40 mils,

$D_{sl}^{(f)} = 315$ mils,

$w_{ant}^{(f)} = 630$ mils,

The complete stripline-fed LTSA structure with complete design values is shown

in Figure 24. The amplitude and phase response of S_{11} obtained using HFSS simulations

for the optimized values of Figure 24 are shown in Figure 25. The optimized $|S_{11}|$ has the

best response with greater than 12 dB return loss. The choice of the circular slotline stub.
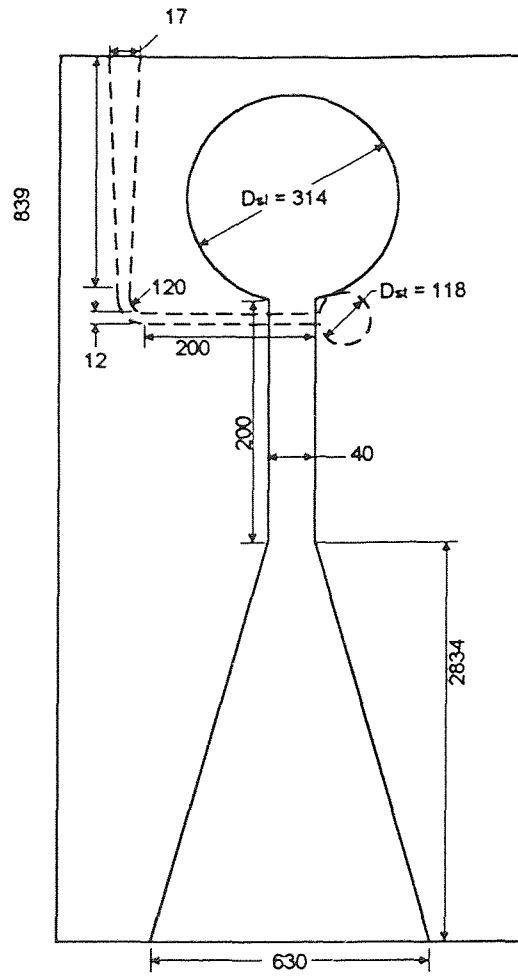
Figure 24. Physical dimensions of the optimized stripline-fed LTSA
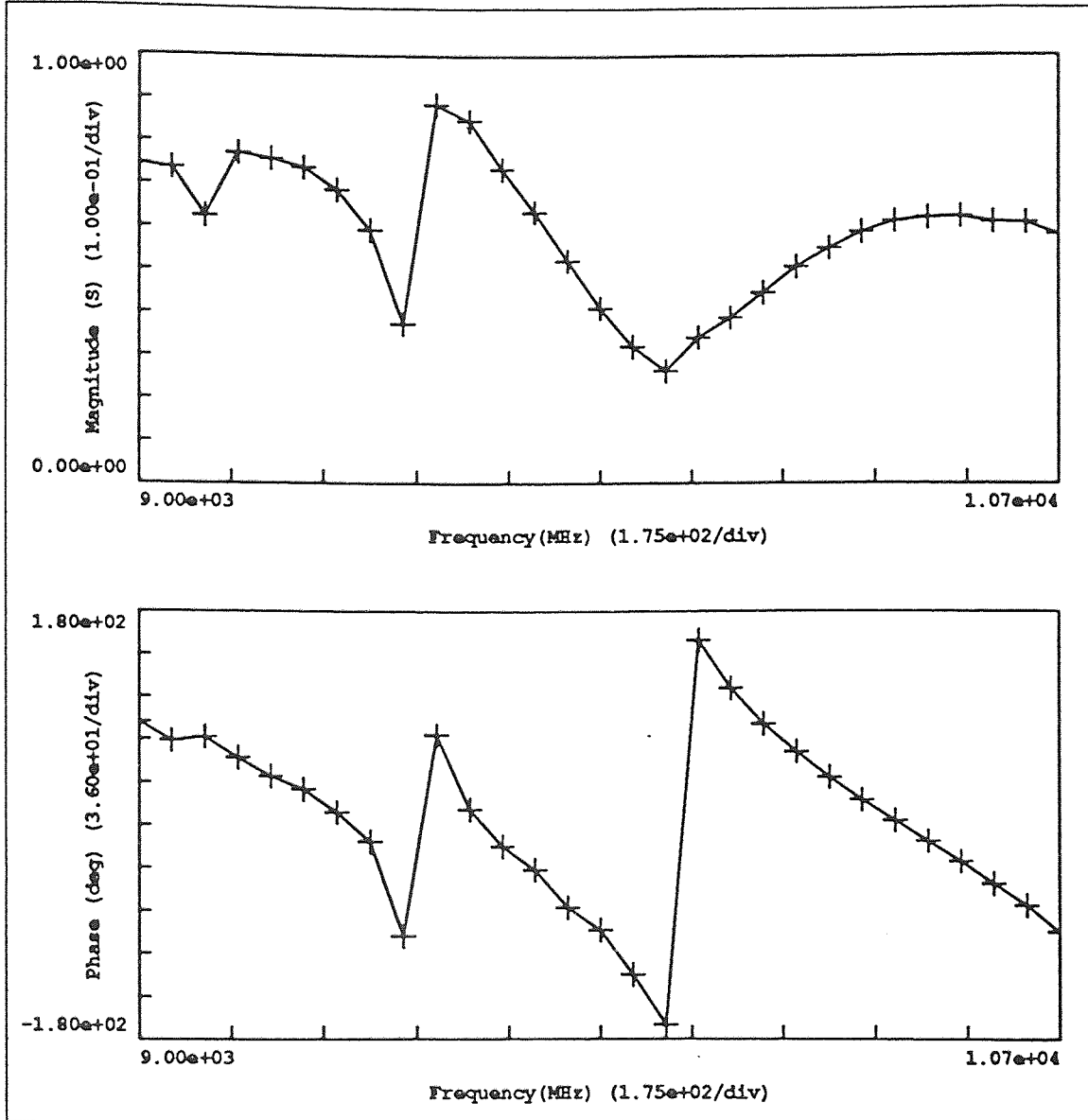
Figure 25. Simulated S11 (both magnitude and phase) of the stripline-fed LTSA.

resulted in obtaining a wider bandwidth as compared to the rectangular slotline stub [36].

Data is limited to a small number of points due to the extensive computational time

required(6 hours per frequency point), even when the number of iterations were kept low

(around 3). Measured results shown in Figure 26 depict a much wider bandwidth of

almost 2 GHz if VSWR < 2 is chosen as an acceptable value. The E-plane radiation

patterns are shown in Figure 27 and 28 for f = 9.9 Ghz and 10.5 Ghz, respectively, and

confirm the endfire radiation characteristics of the designed antenna.

MARKER 1: -25.45 dB (9.59 GHz)
MARKER 2: -9.394 dB (8.00 GHz)
MARKER 3 : -9.89 dB (10.12 GHz)
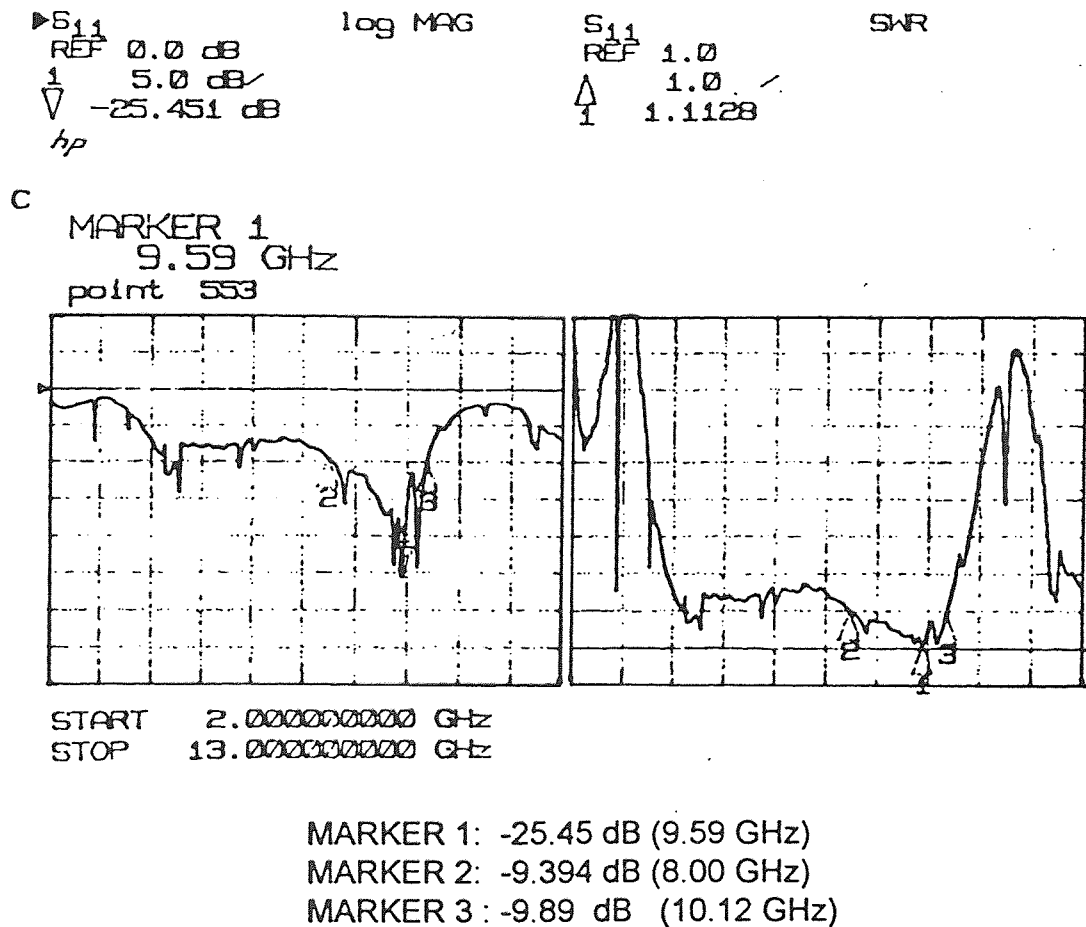
Figure 26. |S11| and SWR of the stripline-fed LTSA
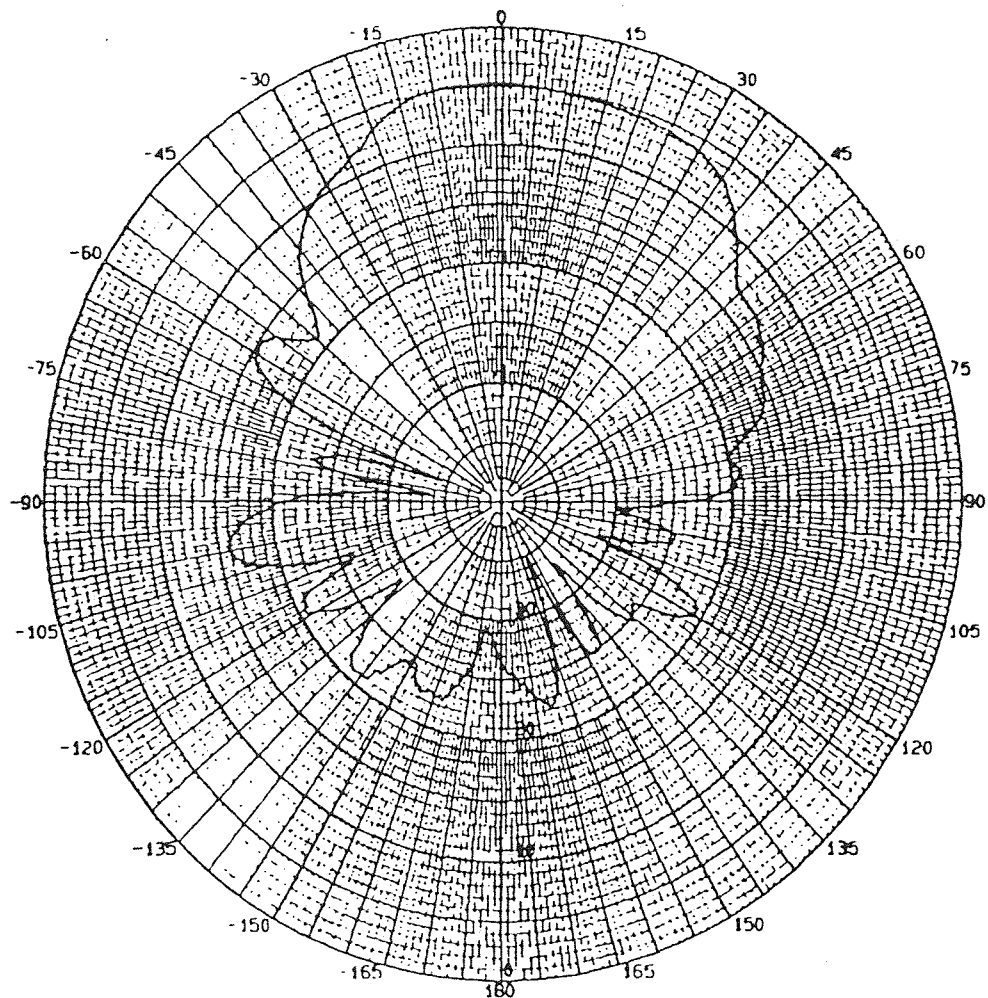
Figure 27. Radiation pattern for the E-plane at 9.9 GHz
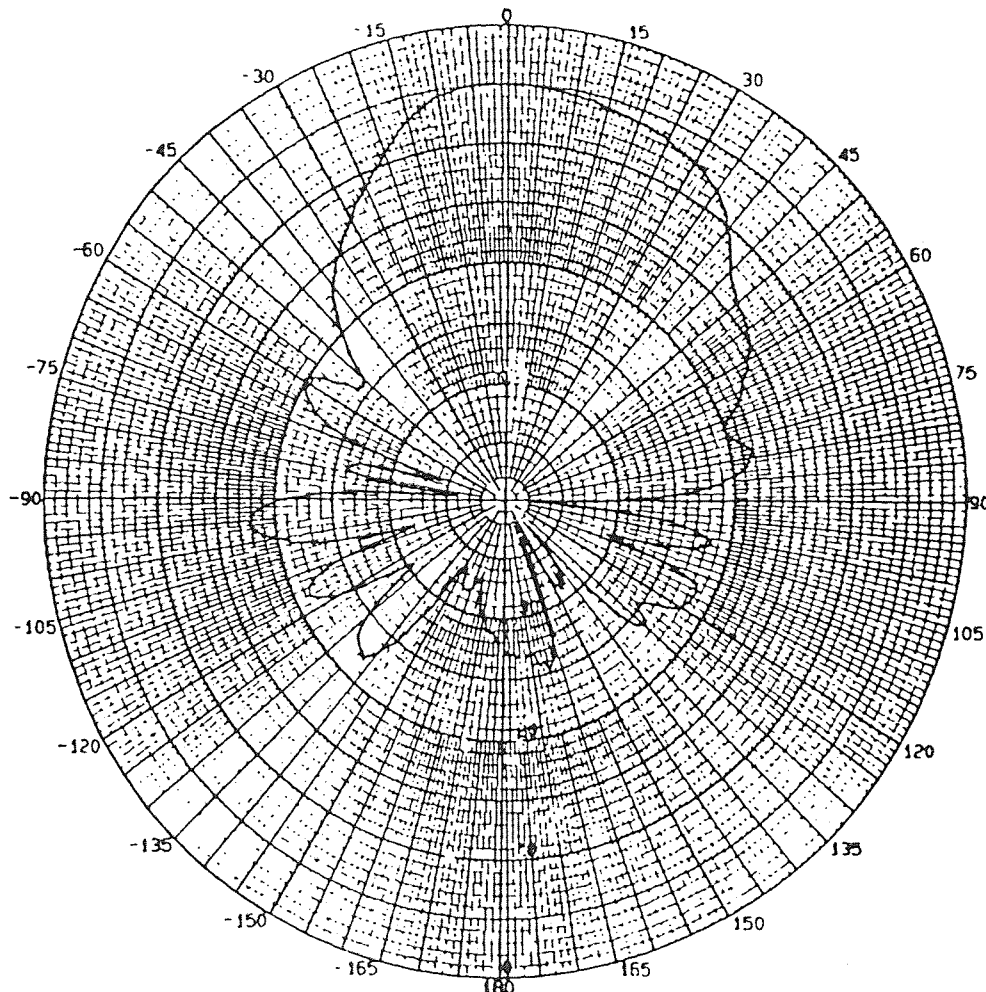
Figure 28. Radiation pattern for the E-plane at 10.5 GHz

5.3 Microstripline-fed LTSA

The microstrip-fed LTSA configuration is simpler to fabricate and does not require extensive alignment needed for stripline-fed LTSA. Only simulation results are presented in this case. The operating frequency is chosen to be 10 Ghz and radial stubs are used in the wideband feed transition (Figure 29).

- Selection of the material

The material chosen for the stripline-fed LTSA are used in this case; therefore, the condition for the optimum range for t_{eff} is already satisfied.

- Design of the antenna

Following the same reasoning used in the previous antenna design, the following dimensions are chosen as initial values:

$$L_{ant}^{(0)} = 2.4\ \lambda_0 = 2834\ \text{mils}.$$

$$2\ \theta = 12°$$

which yield

$$w_{ant}^{(0)} = 2\ L_{ant}\ tg\theta + w_{sl} \approx 613\ \text{mils} \geq \lambda_0 /2 = 590\ \text{mils}.$$

Thus, the value for w_{sl} of 20 mils is obtained in the transition design step.

- Selection and design of the transition

The widths of the uniform sections of the slotline and microstripline are tabulated in Table 3. The initial design values chosen in the design based on Table 3 are
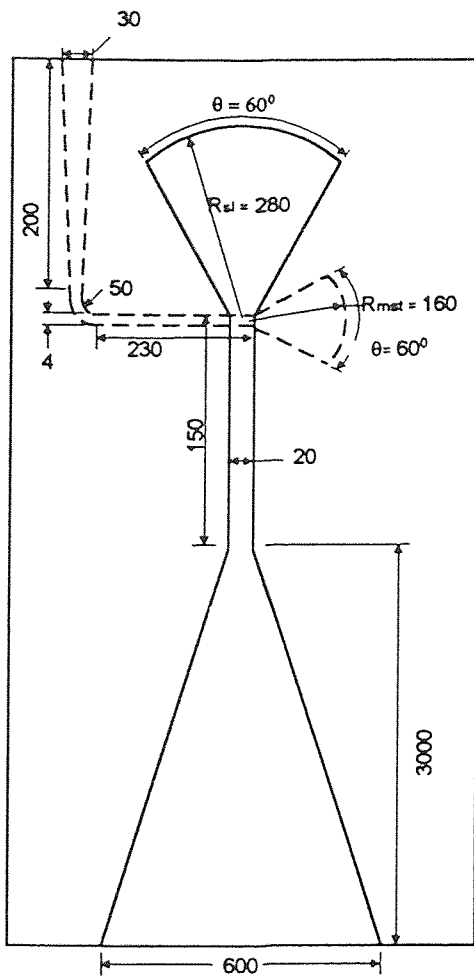
Figure 29. Physical dimensions of microstrip-fed LTSA. (All dimensions are given in mils).

$$w_{sl} = 20 \text{ mils}$$

and

$$w_{mst} = 4 \text{ mils}$$

Table 2 Physical dimensions of the uniform slotline and microstrip transmission, where w_{sl} and w_{mst} are the widths, Z_{sl} and Z_{mst} are the impedances and λ_{sl} and λ_{mst} are the wavelengths for the slotline and microstrip, respectively.

SLOTLINE[1]			MICROSTRIP[2]		
w_{sl}(mils)	Z_{sl}(ohms)	λ_{sl}	w_{mst}(mils)	Z_{mst}(ohms)	λ_{mst}(mils)
40	150	$0.94 \lambda_0$	12	60	796
30	140	$0.93 \lambda_0$	17	50	796

1. Formulae for slotline characteristics for low dielectric were taken from [33] and a program is included in Appendix A.
2. Formulae for stripline characteristics were taken from [35].

In this case, the value for w_{sl} of 20 mils is determined to match the antenna impedance of the LTSA that was chosen as 130 ohms (80-140 ohms). In order to have an optimum match in the transition, the value for the characteristic impedance of the microstrip(Z_{mst}) must have a value of 10 ohms less that the value of the slotline(Z_{sl}) [12]. In this case a good value for Z_{mst} is 120 ohms, which means that W_{mst} has a value of 4 mils. The radial stubs are chosen to have an angle of 60° to avoid strong overlapping that can affect the normal operation of the transition. To design the radial microstrip stub a formula given by [37] is used to determine the radius of the stub, R_{mst}, i.e.,

$$R_{mst} \approx \lambda/(2\pi\sqrt{\varepsilon_{eff}}) \tag{18}$$

The parameters ε_r =2.2, and d=10 mils for the chosen substrate material yield the value for

ε_{eff} of 1.8 (see Table 3). Upon substitution of ε_{eff} ≈ 1.8 in (18) yields a value close to

R_{ms} ≈140 mils. For the design of the radial slotline stub, a program was written and is

included in Appendix B. In this program, the radial stub is divided into N sections and

each section is considered as a transmission line. At the end of these N sections there is a

short circuit termination and at the input there must be a high value of the input impedance

due to the λ/4 transformation of the radial stub. In Table 4, a listing of the output of the

program is presented. It is observed that a value for the radius Rsl ≈280 mils is capable of

providing a high input impedance. With these values of R_{ms}=140 mils and R_{sl}=280 mils a

HFSS simulation was initiated. This was done to ensure that the transition was properly

designed.

Table 4. Listing of output of program RADSTUB.FOR (Appendix B)

θ(degrees)	R_{sl}(mils)	X_{in}(ohms)
60	260	1183.845
60	270	1999.193
60	280	5154.045
60	290	-9635.296
60	300	-2530.111

Different steps taken to assess the transition design are shown in Figure 30. Figure

30(a) depicts a uniform slotline of 20 mils; its simulation produced a value of 134 ohms

for its characteristic impedance. Figure 30(b) tested the validity of using the radial stub by

locating a thin film resistor of 134 ohms between the slotline and the radial stub. The

result was a low $|S_{11}|$ of 0.1. This means that the stub worked as an effective open circuit
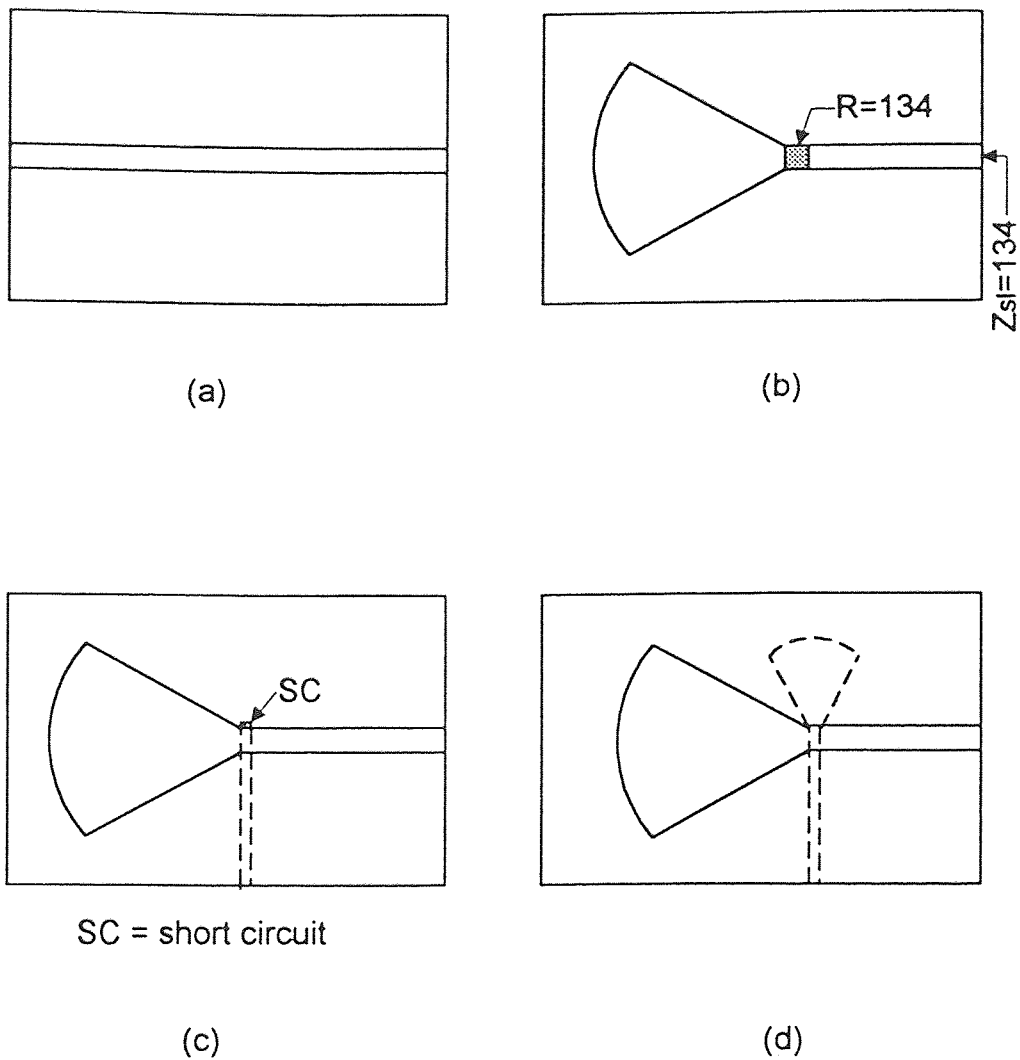
Figure 30. Software tuning of the microstrip-slotline transition (solid line=slot trace; dotted line = microstrip trace.). (a) uniform slotline; (b) virtual open slotline in parallel with resistor; (c) grounded microstrip to slotline; (d) complete transition.

and the slotline was matched by the thin film resistor. In Figure 30(c), the thin film is taken out and a microstrip of 4 mils width is added for a simulation of the transition. In this case a real short circuit was used to tune the transition, which resulted in $|S_{11}| \approx 0.1$. Finally in Figure 30(d) the whole transition is shown, yielding $|S_{11}| \approx 0.15$, this indicates that the design of the transition satisfied the desired matched condition.

- Simulation and Tuning of the Antenna

Using similar procedure as in the stripline-fed LTSA, the microstrip-fed LTSA was simulated. The initial results were not good enough ($|S_{11}| \approx .5$) so the tuning of the antenna was carried out. After some optimization efforts, the length and the aperture of the LTSA were tuned so that it was possible to lower the value of $|S_{11}|$ to 0.25 which was considered to be satisfactory enough. The final dimensions of the antenna were obtained as:

$$L_{ant}^{(f)} = 3000 \text{ mils}$$

$$W_{ant}^{(f)} = 600 \text{ mils} \geq \lambda_0/2 = 590 \text{ mils}$$

The microstrip-fed LTSA antenna shown in Figure 29, depicts the physical values after optimization. The simulation results for S_{11} (both magnitude and phase are shown in Figure 31).
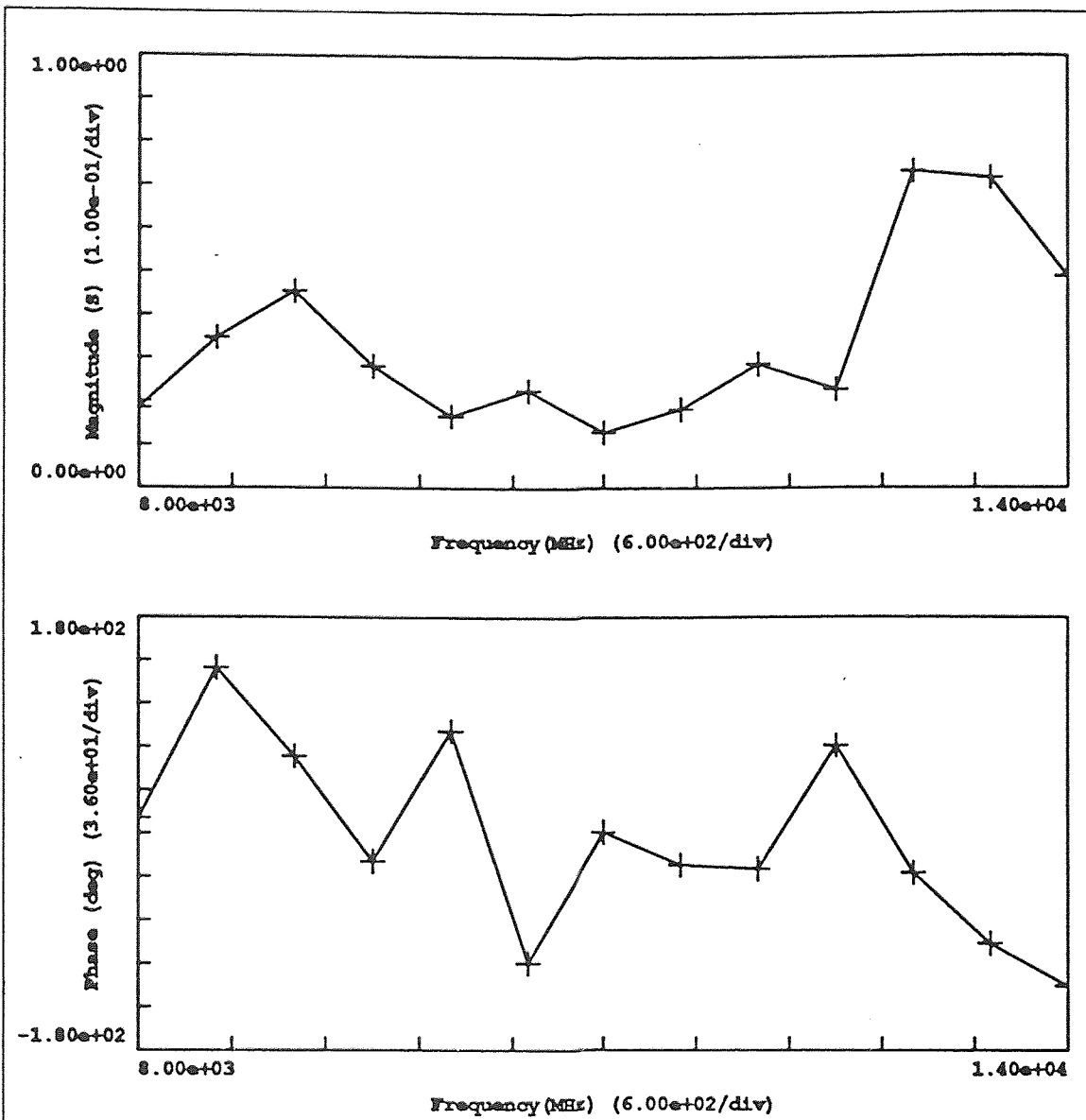
Figure 31. Simulated S11 (both magnitude and phase) of the microstrip-fed LTSA.

CHAPTER 6

CONCLUSIONS

The CAD analysis of the Linear Tapered Slot Antenna (LTSA) requires optimization of a number of parameters to achieve satisfactory operation. Computer codes such as HFSS are adequate for simulations, as validated by experimental observations. Proper choice of the substrate characteristics, design of the radiating and feed structure has to be complemented by additional simulations and optimization to complete the design cycle.

Experimental measurements of the fabricated antenna confirmed that optimization of the microstripline-fed LTSA yields more satisfactory results as compared to the stripline-fed LTSA. Difficulty associated with the stripline-fed LTSA could be conveniently overcome by switching to low temperature co-fired ceramic substrate technology. Designs are being innitiated to realize the LTSA concept in this novel technology. A design of frequency scanning antenna array will be the next step to realize efficient and economic operation in a small volume.

APPENDIX A

PROGRAM FOR DETERMINATION OF SLOTLINE PARAMETERS

```c
/* LDLWSLOT.C*/
/* This program determine the slotline characteristic impedance Z0 and
   the wavelength lambda*/
/* This program is based from the formulae in the paper "Characteristic
   Impedance of a Wide Slotline on Low-permittivity Substrates,"
   by R. Janaswamy and D.H.Schaubert*/
/* The parameters are dielectric permittivity er=2.2, thickness
   of the substrate d=10 mils. The variable is the width of the
   slotline W in mils */
#include <stdio.h>
#include "math.h"
float main()
{
        char inbuf[130];
        float L,W,Z0,er=2.2,d=10,lambda=1181.1,PI=3.14159;
        printf("value of LW([1.83,88.6]mils,er[2.2,3.8])=");
        gets(inbuf);
        sscanf(inbuf,"%f",&W);
        Z0=60+3.69*sin(((er-2.22)*PI)/2.36)
            +133.5*log(10*er)*sqrt(W/lambda)
            +2.81*(1-0.011*er*(4.48+log(er)))*(W/d)*log(100*d/lambda)
            +131.1*(1.028-log(er))*sqrt(d/lambda)
            +12.48*(1+0.18*log(er))*(W/d)/(sqrt(er-2.06+0.85*(W/d)*(W/d)));
        printf("\n The value of Z0 =%f\n", Z0);
        L=1.045 - 0.365*log(er)+6.3*(W/d)*(pow(er,0.945))/(238.64+100*(W/d)) -
          (0.148-8.81*(er+0.95)/(100*er))*log(d/lambda);
        printf("\n The value of LAMBDA =%f\n",L);
        return 0;

}
```

APPENDIX B

PROGRAM FOR DETERMINATION OF INPUT REACTANCE OF A

SLOTLINE RADIAL STUB

```
C  RADSTUB.FOR
C  THIS PROGRAM CALCULATES THE INPUT REACTANCE AT THE INPUT OF
C  A RADIAL SLOTLINE STUB.
C  THIS RADIAL STUB WAS DIVIDED IN N SECTIONS, AND EACH SECTION
C  IS MODELED AS A TRANSMISSION LINE. THE NTH TRANSMISSION LINE
C  HAS A SHORT CIRCUIT AS A TERMINAL LOAD.
C  PARAMETERS ARE: THETA (ANGLE OF THE RADIAL STUB), R(RADIUS OF
C  THE STUB IN MILS), N(TOTAL NUMBER OF SECTIONS), AND THE
C  OUTPUT  IS  ZIN(INPUT  REACTANCE  OF  THE  RADIAL  STUB)
*************************************************************************
*
      REAL H(100),DELTA(100),PI,D1,D2,XOLD1,XOLD2,THETA,ANGLED
      REAL LAMBDAS,LAMBDA0,X,WS,R
      LAMBDA0=1181.1
      D=10.
      ER=2.2
      PI=3.14159
      N1=20
       N2=20
      N=N1+N2
      DO 200 K=3,3
      DO 100 J=1,50
      R=100.+(J-1)*10.
      FREQ=10.
      WSTRIP=20.
      WS=WSTRIP
      ANGLED=50.+(K-1)*5.
      THETA=(PI*ANGLED/180.)
      COSTHETA=COS(THETA/2.)
      D1=(R*COS(THETA/2.)-WS/(2.*TAN(THETA/2.)))/N1
      D2=(R-R*COS(THETA/2.))/N2
      XOLD2=R-D2/2.
      DO 10 I=1,N2
```

```
       X=XOLD2-(I-1)*D2
       H(N+1-I)=2.*SQRT(R*R-X*X)
       XOLD1=X-(D1+D2)/2.
        DELTA(N+1-I)=D2
10     CONTINUE
       DO 20 I=N2+1,N
       X=XOLD1-(I-1-N2)*D1
       H(N+1-I)=2.*X*TAN(THETA/2.)
       DELTA(N+1-I)=D1
20     CONTINUE
       DO 30 I= 1, N
       W=H(N+1-I)
       CALL SLOTPARA(W,LAMBDA0,D,ER,Z0,LAMBDAS,BETAS)
       IF(I.EQ.1) THEN
       ZIN=Z0*TAN(BETAS*DELTA(N+1-I))
       ELSE
        ZIN=Z0*(ZIN+Z0*TAN(BETAS*DELTA(N+1-I)))/(Z0-ZIN*
       *       TAN(BETAS*DELTA(N+1-I)))
        ENDIF
30     CONTINUE
100    WRITE(6,*) ANGLED,R,ZIN
200    CONTINUE
       W=20.
       LAMBDA0=1181.1
       D=10.
       ER=2.2
       CALL SLOTPARA(W,LAMBDA0,D,ER,Z0,LAMBDAS,BETAS)
       WRITE(6,*) Z0,LAMBDAS,BETAS
       W=4.
       STOP
       END
       SUBROUTINE SLOTPARA(W,LAMBDA0,D,ER,Z0,LAMBDAS,BETAS)
       REAL W,LAMBDA0,LAMBDAS,Z0
       PI=3.14159
       IF(W.LE.(0.075*LAMBDA0)) THEN
       LAMBDAS=(0.9217-0.277*LOG(ER) + 0.0322*(W/D)
       *SQRT(ER/(W/D+0.435)) -0.01*LOG(D/LAMBDA0)*(4.6-3.65/
       * (ER*ER*SQRT(W/LAMBDA0)*(9.06-100.*W/LAMBDA0))))*
       * LAMBDA0
       Z0= 73.5 -2.15*ER+(638.9-31.37*ER)*(EXP(0.6*LOG(W/LAMBDA0)))
       *    +(36.23*SQRT(ER*ER+41)-225)*((W/D)/(W/D+0.876*ER-2.))
       *    +0.51*(ER+2.12)*(W/D)*LOG(100.*D/LAMBDA0)
       *    -0.753*ER*(D/LAMBDA0)/(SQRT(W/LAMBDA0))
        ELSE
        LAMBDAS=(1.05-0.04*ER+0.01411*(ER-1.421)*LOG(W/D-2.012*
```

```
*      (1.-0.146*ER))+0.111*(1.-0.366*ER)*SQRT(W/LAMBDA0)
*      +0.139*(1.+0.52*ER*LOG(14.7-ER))*(D/LAMBDA0)*
*      LOG(D/LAMBDA0))*LAMBDA0
 Z0=120.75-3.74*ER+50.*(ATAN(2.*ER)-0.8)*
*  EXP((1.11+(0.132*(ER-27.7)/(100.*D/LAMBDA0+5.)))*LOG(W/D))
*  *LOG(100.*D/LAMBDA0+SQRT((100.*D/LAMBDA0)*
*   (100.*D/LAMBDA0)+1)) + 14.21*(1.-0.458*ER)*(100.
*   D/LAMBDA0+5.1*LOG(ER)-13.1)*(W/LAMBDA0+0.33) *
*   (W/LAMBDA0+0.33)
 ENDIF
 BETAS=2.*PI/LAMBDAS
 RETURN
 END
```

REFERENCES

[1]   Korzeniowski, T.L., D.M. Pozar, D.H. Schaubert, and K.S. Yngvesson, "Imaging system at 94 Ghz using tapered slot antenna elements," Proc. 8th Int. Conf. Infrared Millimeter Waves (1983).

[2]   Wang, N., S.E. Schwarz, and T. Hierl, "Monolithically integrated Gunn oscillator at 35 Ghz," Electron. Lett. 20 (1984): 603-604.

[3]   Rascoe, D., et al., "Ka-band MMIC beam steered planar array feed," MTT-S Int. Microwave Symp. Dig. (1990): 809-812.

[4].   Collin, R.E., F.J. Zucker, "General characteristics of traveling-wave antennas," *Antenna Theory*. 19 (1969): New York: McGraw-Hill.

[5].   Barlow, H.M., and J. Brown, 1962. *Radio Surface Waves*. Fair Lawn, N.J.:Oxford.

[6].   Walter, C.H., "Synthesis of continuous source distributions," *Traveling-wave antennas*. 3 (1965): New York: Dover, Inc.

[7]   Hansen, W.W., and J.R. Woodyard, "A New principle in antenna design," Proc. IRE. (1938): 333 - 345.

[8]   Ehrenspeck, H.W., and H. Poehler, "A new method for obtaining maximum gain from Yagi antennas," IRE Trans. Antennas Propagat. 7 (1959): 379.

[9]   Zucker, F.J., "Surface-wave antennas,". *Antenna Engineering Handbook*. 12 (1993): New York : McGraw-Hill.

[10]   Kobayashi, S., R. Mittra, and R. Lampe, "Dielectric tapered rod antennas for millimeter-wave application," IEEE Trans.Antennas Propagat. 30 (1981): 54-58.

[11]   Yngvesson, K.S., D.H. Schaubert, T.L. Korzeniowski, Y.S. Kim, E.L. Kollberg, and J.F. Johanson, "The tapered slot antenna -a new integrated element for millimeter-wave applications," IEEE Trans. Microwave Theory Tech. 37 (1989): 364-374.

[12]   Knorr, J.B.,"Slot-line transitions," IEEE Trans. Microwave Theory Tech. 22 (1974): 548-554.

[13]   Mariani, E.A., C.P. Heinzman, J.P. Agrios, and S.B. Cohn, "Slot line characteristics," IEEE Trans. Microwave Theory Tech. 17 (1969): 1091-1096.

[14] Robinson, G.H., and J.L. Allen, "Slot line application to miniature ferrite devices," IEEE Trans. Microwave Theory Tech. 17 (1969): 1097-1101.

[15] de Ronde, F.C., "A new class of microstrip directional couplers," Dig. G-MTT Symp. (1970): 184 -189.

[16] Schiek, B., and J. Koehler, "An improved microstrip-to-microslot transition," IEEE Trans. Microwave Theory Tech. 24 (1976): 231-233.

[17] Schuppert, B.,"Microstrip/slotline transitions: modeling and experimental investigation," IEEE Trans. Microwave Theory Tech. 36 (1988): 1272-1282.

[18] Schuppert, B., "Analysis and design of microwave balanced mixers," IEEE Trans. Microwave Theory Tech. 34 (1986): 120-128.

[19] Yang, H., and N. Alexopoulos, "A Dynamical model for microstrip-slotline transition and related structures," IEEE Trans. Microwave Theory Tech. 36 (1988): 286-293.

[20] Dib, Nihad I., Rainee N. Simons, and Linda P.B. Katehi, "Broadband uniplanar microstrip to slot-line transitions," Dig. Int. Microwave Symp. (1995): 683-686.

[21] Stephenson, B.T., and C.H. Walter, "Endfire slot antennas," IEEE Trans.Antennas Propagat. 3 (1955): 81-86.

[22] Eberle, J.W., C.A. Lewis, and D.M. McCoy, "The flared slot: a moderately directive flush-mounted broad-band antenna," IRE Transact. on Antennas and Propagt. (1960): 461-468.

[23] Gibson, P.J., "The Vivaldi aerial," Dig. of 9th Eur. Microw. Conf. (1979): 120-124.

[24] Stutzman, W.L., and G.A. Thiele, " Wire Antennas," *Antenna Theory and design* (1981). New York: John Wiley & Sons.

[25] Thungren, T., E.L. Kollberg, and K.S. Yngvesson, "Vivaldi antennas for single beam integrated receivers," Dig. of 12th Eur. Microw. Conf. (1982).

[26] Carrel, R., "The characteristic impedance of two infinite cones of arbitrary cross section," IEEE Trans.Antennas Propagat. 6 (1958): 197-201.

[27] Yngvesson, K.S., et al., "Endfire tapered slot antennas in dielectric substrates," IEEE Trans. Antennas Propagat. 33 (1985): 1392-1400.

[28]   Prasad, S.N. , and S. Mahapatra " A novel MIC slotline antenna," Dig. of 9th Eur. Microw. Conf. (1979): 120-124.

[29]   Yngvesson, K.S., J.F. Johansson, and E.L. Kollberg, "A new integrated slot element feed array for multibeam systems," IEEE Trans.Antennas Propagat. 34 (1986): 1372-1376.

[30]   Acharya, P.R., J. Johansson, and E.L. Kollberg, "Slotline antennas for millimetre and sub millimetre wavelength," Dig. of 20th Eur. Microw. Conf. (1990): 353-358.

[31]   Courant, R.L., "Variational method for the solution of problems of equilibrium and vibration" Bulletin of the American Mathematical Society 49 (1943): 1-23.

[32]   Shenton, D.N., and Z.J. Cendes, "Three-dimensional finite element mesh generation using Delaunay tessellation," IEEE Trans. Magn. 21 (1985):2535-2538.

[33]   Janaswamy, R., and D.H. Schaubert, "Characteristic impedance of a wide slotline on low-permittivity substrates," IEEE Trans. Microwave Theory Tech. 34 (1986): 900-902.

[34]   Rebeiz, G.M. "Millimeter-wave and Terahertz integrated circuit antennas." Proc. of the IEEE 80 (1992): 1748-1770

[35]   Hoffmann, R.K., "Microstrip-Line Variations," Handbook of Microwave Integrated Circuits (1987).Norwood, MA: Artech House.

[36]   Kwan, A., "CAD study of linear tapered slot antenna," M.Sc. Thesis, NJIT, 1994.

[37]   Atwater, H. A., "Microstrip reactive circuit elements," IEEE Trans. Microwave Theory Tech. 31 (1983): 488 - 491.